Lunar meteorite regolith breccias: An in situ study of impact melt composition using LA-ICP-MS with implications for the composition of the lunar crust

Journal Article

The Meteoritical Society

Meteoritics & Planetary Science 45, Nr 6, 917–946 (2010)
doi: 10.1111/j.1945-5100.2010.01067.x

Lunar meteorite regolith breccias: An in situ study of impact melt composition using LA-ICP-MS with implications for the composition of the lunar crust

Katherine H. JOY[1,2,3,4*], Ian A. CRAWFORD[1,5], Sara S. RUSSELL[2], and Anton T. KEARSLEY[2]

[1]The Centre for Planetary Science, The Joint UCL/Birkbeck Research School of Earth Sciences, Gower Street, London, WC1E 6BT, UK
[2]The Department of Mineralogy, The Natural History Museum, Cromwell Road, London SW7 5BD, UK
[3]Center for Lunar Science and Exploration, The Lunar and Planetary Institute-USRA, 3600 Bay Area Boulevard, Houston, Texas 77058, USA
[4]The NASA Lunar Science Institute
[5]Department of Earth and Planetary Sciences, Birkbeck College, London, WC1E 7HX, UK
[*]Corresponding author. E-mail: joy@lpi.usra.edu

(Received 04 March 2009; revision accepted 05 April 2010)

Abstract–Dar al Gani (DaG) 400, Meteorite Hills (MET) 01210, Pecora Escarpment (PCA) 02007, and MacAlpine Hills (MAC) 88104/88105 are lunar regolith breccia meteorites that provide sampling of the lunar surface from regions of the Moon that were not visited by the US Apollo or Soviet Luna sample return missions. They contain a heterogeneous clast population from a range of typical lunar lithologies. DaG 400, PCA 02007, and MAC 88104/88105 are primarily feldspathic in nature, and MET 01210 is composed of mare basalt material mixed with a lesser amount of feldspathic material. Here we present a compositional study of the impact melt and impact melt breccia clast population (i.e., clasts that were generated in impact cratering melting processes) within these meteorites using in situ electron microprobe and LA-ICP-MS techniques. Results show that all of the meteorites are dominated by impact lithologies that are relatively ferroan ($Mg\#_{<70}$), have high Sc/Sm ratios (typically >10), and have low incompatible trace element (ITE) concentrations (i.e., typically <3.2 ppm Sm, <1.5 ppm Th). Feldspathic impact melt in DaG 400, PCA 02007, and MAC 88104/05 are similar in composition to that estimated composition for upper feldspathic lunar crust (Korotev et al. 2003). However, these melt types are more mafic (i.e., less Eu, less Sr, more Sc) than feldspathic impact melts returned by the Apollo 16 mission (e.g., the group 3 and 4 varieties). Mafic impact melt clasts are common in MET 01210 and less common in PCA 02007 and MAC 88104/05. We show that unlike the Apollo mafic impact melt groups (Jolliff 1998), these meteorite impact melts were not formed from melting large amounts of KREEP-rich (typically >10 ppm Sm), High Magnesium Suite (typically >70 Mg#) or High Alkali Suite (high ITEs, Sc/Sm ratios <2) target rocks. Instead the meteorite mafic melts are more ferroan, KREEP-poor and Sc-rich, and represent mixing between feldspathic lithologies and low-Ti or very low-Ti (VLT) basalts. As PCA 02007 and MAC 88104/05 were likely sourced from the Outer-Feldspathic Highlands Terrane our findings suggest that these predominantly feldspathic regions commonly contain a VLT to low-Ti basalt contribution.

INTRODUCTION

Lunar regolith is defined as a layer or mantling deposit that that has been generated from continual meteoroid bombardment of bedrock lithological units (McKay et al. 1991). This physical modification causes the shattering, disaggregation, pulverization, melting, transporting, and mixing of lithic and mineral fragments, forming a poorly consolidated layer on the lunar surface (Hörz et al. 1991). Typically this layer is much less than 1 cm in grain size, although very large boulders and cobbles are commonly strewn across the

lunar surface. The lunar regolith provides a record both of the Moon's geological history and its interaction with the dynamic inner solar system space environment (Lucey et al. 2006). This archive is important for our understanding of the evolution of terrestrial planets, as few other planets (such as the Earth, Mars, and Venus) have retained such a complete record of their earliest history.

Lunar regolith breccia meteorites are consolidated samples of the lunar regolith that were ejected from the Moon and transported to Earth by impact cratering processes. They have potentially been launched from anywhere on the lunar surface, although their precise launch craters are unknown. These meteorites reflect a broad range of compositional affinities from different lunar lithological terranes (Korotev 2005), including the feldspathic highlands (likely from both the far and nearside regions); from basaltic lavas; from areas formed from mixtures of basalt and feldspathic bedrock; and also from environments dominated by KREEP-rich impact melts (i.e., samples characterized by high concentrations of potassium, rare earth elements, and phosphorus).

Radiogenic isotope studies indicate that the majority of known lunar meteorites have been launched from the Moon in the last 10 million years (Korotev 2005), and all have been launched in the last 20 million (Nishiizumi and Caffee 2001). As there are believed to have been no large craters formed on the Moon during this period (all craters in the last 1 million years or so are <3.6 km in diameter; Warren 1994), it is assumed that all lunar meteorites must therefore be launched from small craters only a few kilometers or less in diameter (Head et al. 2002). Moreover, evidence from studies of cosmic-ray exposure indicates that many of the regolith breccia samples have been preferentially derived from very shallow to shallow stratigraphic horizons (2 m to <100 m; Warren 1994). For this reason they can provide a valuable calibration for the composition of the upper regolith, especially for inaccessible farside geological terranes (Korotev et al. 2006). For example, lunar feldspathic regolith breccia meteorites have been used to help calibrate remote sensing information from the lunar feldspathic highlands (Warren 2005; Joy et al. 2006a; Prettyman et al. 2006; Swinyard et al., 2009), and have been used to inform discussions of lunar anorthositic primary crust petrogenesis and evolution (Palme et al. 1991; Jolliff and Haskin 1995; Shearer and Floss 2000; Korotev et al. 2003; Longhi 2003; Warren et al. 2005).

Lunar regolith breccias are polymict fragmental rocks, containing components that are characteristic of the lunar soil (defined by McKay et al. 1991 as "the sub-centimeter fraction of the lunar regolith" formed of very fine grained (average grain size between 60 and 80 μm clastic and mineral material). These regolith components include impact melt spherules (melt beads), impact glass, agglutinates (unique glassy bonded soil particles containing an impact derived nanophase Fe component; Taylor et al. 1991), an exogenous meteoritic component (Rubin 1997; Zolensky 1997; Day et al. 2006), and clasts of older breccias. The presence of just one or a combination of several of these components is evidence that the breccia was fused together in a lunar regolith environment. Estimates of the maturity of this regolith environment (i.e., how long it was exposed to space) is inferred from bulk sample grain size (generally mature soils are finer grained and have more agglutinate particles) and surface exposure ages (i.e., length of time it was exposed to ionizing radiation; Lucey et al. 2006). Igneous rock and mineral fragments form a significant component of regolith breccias, and the modal mineralogy, mineral composition, and bulk composition of these clasts can be used to construct an inventory of their bedrock source lithologies. This inventory can then be used to interpret the petrological history of individual clasts and provide new information about global lunar magmatic processes and geological variation (e.g., Nyquist et al. 2006).

Lunar regolith breccias commonly contain clasts of impactite rocks derived from rock that was recrystallized, partially melted or completely melted by meteorite impacts (see discussion by Cohen et al. 2004). These impactites represent a compositional mixture of all the rocks types that were located in the target area and commonly also contain a minor additional contribution from the impacting bolide body. Thus, the products of meteorite impacts (melts and metamorphites) can commonly be distinguished from indigenous igneous products (and their metamorphites) by their siderophile elements abundances, where impact material will be relatively rich in siderophiles, derived from meteoritic impactors (Warren and Wasson 1977, 1978). Impact lithologies are an important indicator of geochemical and lithological provenance as their compositions provide an insight into the nature of local geological terranes. For example, the low-K Fra Mauro ("LKFM") mafic impact melts (Spudis et al. 1991; Korotev 2000), returned from the Apollo 15 landing site (i.e., samples 15445 and 15455, Ryder and Spudis 1994), are thought to have been formed during the Imbrium basin impact (Spudis 1993). As these mafic impact melts were returned from a known locality on the lunar nearside, it can be assumed that this reflects a geochemical signature directly related to basin forming within the Procellarum KREEP Terrane ("PKT"; Jolliff et al. 2000; Haskin et al. 2000; Korotev 2000), and is perhaps indicative of the nature of the lower near-side

crust (approximately 40 to 80 km depth: Spudis 1993). Impact melt and breccia clasts therefore are important micro-samples to study in regolith breccias as they preserve a compositional record of crustal terranes from regions not sampled by the Apollo and Luna sample return missions.

SAMPLES AND ANALYTICAL METHODS

We were loaned a polished thick section block of DaG 400 ($8.5 \times 6.8 \times 1$ mm) from the Vatican Observatory Collection. The sample had previously been used for trace element investigations by LA-ICP-MS (laser ablation inductively coupled mass spectrometry) and so there was some scarring by laser pits and ablated ejecta (see Consolmagno et al. [2004] for details of this prior study). In order to gain precise quantitative reproducible results, microprobe measurements were not taken from areas within 150 μm of these pre-existing laser pits and the section was repolished to remove as much deposited material as possible before we started our analysis. In addition, a small portion of DaG 400 (200 mg) was removed from a large slab held at the Natural History Museum London (NHM) for use in bulk composition analysis (Table 1).

We also studied polished carbon coated thick-thin sections of MET 01210,21 ($10.4 \times 14.6 \times 0.2$ mm), MET 01210,27 ($8.6 \times 13.1 \times 0.2$ mm), PCA 02007,34 ($14 \times 6.8 \times 0.2$ mm), MAC 88104,47 ($10 \times 8 \times 0.2$ mm), and MAC 88105,159 ($11 \times 6 \times 0.2$ mm) (Fig. 1) and used chip sub-splits of MET 01210,25, PCA 02007,37, MAC 88104,45, MAC 88105,106, and homogenous powder sub-split MAC 88105,41 (Lindstrom et al. 1991) for bulk composition analysis (Table 1). We determined the bulk-rock major, minor, and trace-element composition of powdered chips of the meteorites by inductively coupled plasma—atomic emission spectrometry (ICP-AES) and mass spectrometry (ICP-MS) at the NHM using the techniques and instrumental setup described by Joy et al. (2008). The instruments used were a Varian VISTA PRO Axial ICP-AES and a Varian ICP-MS. Comparison between our elemental values and literature meteorite compositions are discussed in section Constraining the Source Region of DaG 400, MET 01210, PCA 02007, and MAC 88104/05.

We determined the major and minor element concentrations of the mineral phases present in these sections using a Cameca SX50 wavelength dispersive electron microprobe (EMP) at the NHM. For silicate, sulfide and metal analysis the Cameca was operated at a 20 keV accelerating voltage with a 20 nA beam current with a focused beam analysis for 10 to 30 s count time per element. X-ray maps and clast bulk composition analyses were made by energy dispersive spectrometry using a JEOL 5900LV SEM at the NHM, fitted with an Oxford Instruments INCA energy dispersive spectrometer (EDS) X-ray microanalyzer system and operated at a 20 keV accelerating voltage and 2 nA beam current. All WDS and EDS investigations employed well characterized natural and synthetic standards as used in previous studies by Joy et al. (2006b, 2008).

Clast Bulk Composition Methodology

We identified and classified impact lithologies according to the textural classifications of Stöffler et al. (1980) where impact melt is defined as clast poor with a glassy or crystalline matrix, and impact melt breccias are defined as clast rich breccia with either a particulate, glassy or clastic matrix.

Major Elements

Many impact melt and impact melt breccia clasts are cracked and/or very fine grained and it is difficult to directly measure spot points of individual mineral and glass phases using EMP analysis. As such, it is challenging to consistently calculate every bulk clast composition using a modal recombination technique or by using an average of matrix-corrected gridded spot analyses. We therefore chose to estimate clast major element composition using an EDS digitally controlled raster beam analysis (RBA). Several RBA were made for each clast, from the same region of interest (for the exact numbers of analyses per clast please refer to Table S1). X-ray spectra were collected from each digitized pixel of a selected region (polygon) of the clast, avoiding where possible pore spaces, fractures that were potentially infilled with terrestrial contaminants, surface contaminants etc. The accumulated X-ray counts were added together and in-built system matrix corrections performed on the total counts to derive element atomic abundances. Analytical errors per element for a single RBA analysis are < 0.05 wt% (1σ) and typically < 0.02 wt% (1σ). We ensured that reported element values were above instrument detection limits. Bulk clast composition was derived by first normalizing the results to 100% to minimize low totals caused by void spaces, mineral edge effects and small fractures and then averaging the repeat analyses together. The relative standard deviation (one standard deviation of repeat RBA measurements expressed as a percentage of their mean value) for oxides with > 5 wt% (e.g., SiO_2, Al_2O_3, CaO, MgO, FeO) is typically 0.3–2%. For oxides with 0.5–5 wt% (e.g., MgO, FeO, TiO_2) the relative standard deviation ranges from 5–10%. For oxides with < 0.5 wt% relative standard deviation is typically >20% and for K_2O, Cr_2O_3, and

Table 1. Bulk composition of DaG 400, PCA 02007, MET 01210, and MAC 88104/05 as measured by our study. (DaG 400, PCA 02007, and MET 01210 compositions were preliminarily reported by Joy et al. 2006a; and MET 01210 composition was also reported in Joy et al. 2008). Errors are shown to 2σ based on repeat analysis of each sample. Most oxide major elements, Cr^1, Sr^1, and Ba measured by ICP-AES with three repeated analyses. Trace elements and P_2O_5 measured by ICP-MS with five repeated analyses. b.d. = below detection limits and n.m. = element not measured.

	DaG 400	PCA 02007	MET 01210		MAC 88104	MAC 88105	
		PCA 02007,37	MET 01210,25	MET 01210,27	MAC 88104,45	MAC 88105,106	MAC 88105,41
SiO_2	41.42 ± 0.26	43.41 ± 0.28	44.03 ± 0.30	44.62 ± 1.98	45.63 ± 0.20	45.02 ± 0.30	44.24 ± 0.28
TiO_2	0.173 ± 0.002	0.28 ± 0.06	1.55 ± 0.01	1.66 ± 0.43	0.246 ± 0.001	0.221 ± 0.001	0.235 ± 0.004
Al_2O_3	27.76 ± 0.10	25.71 ± 0.15	16.60 ± 0.09	14.86 ± 5.91	28.95 ± 0.74	29.30 ± 0.24	29.24 ± 0.50
Cr_2O_3	0.08 ± 0.001	0.171 ± 0.002	0.28 ± 0.02	0.24 ± 0.11	0.089 ± 0.001	0.083 ± 0.001	0.100 ± 0.001
FeO	3.61 ± 0.08	6.30 ± 0.13	16.46 ± 0.64	17.68 ± 4.42	4.59 ± 0.03	4.318 ± 0.000	4.39 ± 0.04
MnO	0.069 ± 0.002	0.085 ± 0.002	0.22 ± 0.02	0.26 ± 0.08	0.068 ± 0.001	0.061 ± 0.001	0.061 ± 0.001
MgO	4.84 ± 0.04	6.80 ± 0.04	6.20 ± 0.05	6.96 ± 1.79	4.26 ± 0.05	4.25 ± 0.02	4.13 ± 0.08
BaO	1.34						
CaO	17.24 ± 0.24	15.19 ± 0.15	12.96 ± 0.22	12.86 ± 1.22	16.32 ± 0.09	16.14 ± 0.08	16.12 ± 0.21
Na_2O	0.387 ± 0.002	0.357 ± 0.002	0.32 ± 0.02	0.29 ± 0.15	0.303 ± 0.001	0.297 ± 0.003	0.309 ± 0.002
K_2O	0.077 ± 0.002	0.031 ± 0.002	0.06 ± 0.02	0.06 ± 0.03	0.117 ± 0.001	0.022 ± 0.001	0.029 ± 0.001
P_2O_5	0.434 ± 0.003	0.026 ± 0.002	0.13 ± 0.02	0.06 ± 0.03	0.037 ± 0.001	0.026 ± 0.001	0.032 ± 0.001
Total	97.43	98.37	98.81	99.54	100.60	99.74	98.89
Mg #	70.48	65.82	40.20	41.27	62.35	63.69	62.69
Sc^1	6.52 ± 0.01	12.75 ± 0.09	55.86 ± 0.02	n.m.	9.47 ± 0.26	8.33 ± 0.04	8.58 ± 0.14
Sc^2	5.68 ± 0.37	11.45 ± 0.57	53.43 ± 0.56	n.m.	n.m.	n.m.	n.m.
V	18.1 ± 0.2	32.5 ± 0.1	59.8 ± 0.3	n.m.	20.3 ± 0.5	17.6 ± 0.2	17.3 ± 0.2
Cr^1	527 ± 8	1168 ± 10	1881 ± 32	n.m.	606 ± 2	566 ± 4	686 ± 6
Cr^2	432 ± 3	941 ± 3	1708 ± 10	n.m.	n.m.	n.m.	n.m.
Co	15.3 ± 0.2	27.1 ± 0.5	31.8 ± 0.2	n.m.	17.0 ± 0.4	16.4 ± 0.1	15.6 ± 0.2
Ni	143 ± 3	324 ± 2	212 ± 4	n.m.	134 ± 2	133 ± 1	147 ± 5
Cu	15.6 ± 0.2	11.2 ± 0.0	23.4 ± 0.1	n.m.	5.5 ± 0.8	6.0 ± 0.8	5.1 ± 0.1
Zn	5.4 ± 0.1	16.9 ± 0.2	37.4 ± 0.1	n.m.	14.9 ± 0.4	15.6 ± 0.1	12.9 ± 0.2
Ga	3.7 ± 0.2	3.1 ± 0.2	19.1 ± 0.4	n.m.	3.5 ± 0.1	3.9 ± 0.1	4.3 ± 0.1
Rb	0.88 ± 0.07	0.59 ± 0.16	1.34 ± 0.15	n.m.	1.19 ± 0.10	1.03 ± 0.03	1.00 ± 0.03
Sr^1	451 ± 7	144 ± 1	163 ± 1	n.m.	n.m.	n.m.	n.m.
Sr^2	440 ± 35	136 ± 8	164 ± 9	n.m.	169 ± 2	161 ± 1	163 ± 4
Y	9.6 ± 0.1	10.6 ± 0.1	36.8 ± 0.1	n.m.	12.6 ± 0.5	10.5 ± 0.1	10.9 ± 0.1
Zr	39.9 ± 0.4	58.2 ± 2.4	102.8 ± 1.4	n.m.	44.8 ± 2.9	36.1 ± 2.5	34.0 ± 3.9
Nb	2.26 ± 0.21	2.64 ± 0.20	1.07 ± 0.07	n.m.	2.85 ± 0.33	2.62 ± 0.21	2.88 ± 0.12
Mo	0.94 ± 0.08	0.41 ± 0.05	12.84 ± 0.31	n.m.	0.062 ± 0.005	0.06 ± 0.01	0.21 ± 0.04
Cd	0.16 ± 0.02	0.11 ± 0.03	0.25 ± 0.05	n.m.	n.m.	n.m.	n.m.
Cs	0.022 ± 0.004	0.047 ± 0.008	0.089 ± 0.015	n.m.	0.075 ± 0.002	0.051 ± 0.005	0.038 ± 0.002
Ba	1203 ± 3	70.2 ± 0.4	80.8 ± 0.3	n.m.	32.9 ± 0.2	28.0 ± 0.2	30.0 ± 0.4
La	3.52 ± 0.20	2.52 ± 0.09	6.69 ± 0.21	n.m.	2.87 ± 0.26	2.77 ± 0.22	2.82 ± 0.13
Ce	7.62 ± 0.35	6.21 ± 0.22	13.81 ± 0.41	n.m.	7.18 ± 0.63	6.60 ± 0.48	7.31 ± 0.38
Pr	1.07 ± 0.04	0.89 ± 0.02	2.12 ± 0.12	n.m.	1.04 ± 0.08	1.00 ± 0.06	1.02 ± 0.08
Nd	4.85 ± 0.06	4.19 ± 0.18	10.66 ± 0.54	n.m.	4.58 ± 0.33	4.44 ± 0.24	4.34 ± 0.08
Sm	1.33 ± 0.06	1.22 ± 0.06	3.58 ± 0.11	n.m.	1.31 ± 0.08	1.26 ± 0.07	1.29 ± 0.09
Eu	1.02 ± 0.06	0.88 ± 0.05	1.11 ± 0.06	n.m.	0.84 ± 0.06	0.91 ± 0.06	0.93 ± 0.01
Gd	1.48 ± 0.09	1.44 ± 0.12	4.54 ± 0.32	n.m.	1.56 ± 0.13	1.50 ± 0.06	1.70 ± 0.01
Tb	0.27 ± 0.02	0.29 ± 0.01	0.91 ± 0.05	n.m.	0.29 ± 0.01	0.28 ± 0.03	0.30 ± 0.02
Dy	1.62 ± 0.15	1.81 ± 0.09	5.85 ± 0.31	n.m.	1.91 ± 0.13	1.85 ± 0.12	1.85 ± 0.12
Ho	0.34 ± 0.02	0.39 ± 0.01	1.26 ± 0.07	n.m.	0.40 ± 0.02	0.39 ± 0.02	0.41 ± 0.02
Er	1.00 ± 0.06	1.16 ± 0.03	3.63 ± 0.14	n.m.	1.19 ± 0.06	1.17 ± 0.03	1.20 ± 0.08
Tm	0.14 ± 0.01	0.16 ± 0.01	0.53 ± 0.03	n.m.	0.17 ± 0.01	0.16 ± 0.01	0.18 ± 0.02
Yb	0.90 ± 0.01	1.11 ± 0.05	3.54 ± 0.10	n.m.	1.15 ± 0.10	1.10 ± 0.05	1.11 ± 0.10
Lu	0.13 ± 0.02	0.164 ± 0.003	0.52 ± 0.02	n.m.	0.15 ± 0.01	0.15 ± 0.01	0.17 ± 0.01
Hf	0.69 ± 0.09	0.83 ± 0.06	2.37 ± 0.10	n.m.	0.91 ± 0.03	0.81 ± 0.06	0.95 ± 0.06
Ta	0.20 ± 0.08	0.18 ± 0.03	0.10 ± 0.02	n.m.	0.14 ± 0.01	0.12 ± 0.01	0.18 ± 0.06
W	b.d.	0.19 ± 0.08	0.69 ± 0.21	n.m.	0.09 ± 0.01	0.068 ± 0.003	0.15 ± 0.15
Th	0.39 ± 0.03	0.37 ± 0.02	0.86 ± 0.03	n.m.	0.53 ± 0.01	0.48 ± 0.01	0.45 ± 0.01
U	0.47 ± 0.04	0.11 ± 0.01	0.32 ± 0.02	n.m.	0.13 ± 0.01	0.12 ± 0.01	0.13 ± 0.01
Li	6.22 ± 0.03	3.75 ± 0.02	8.07 ± 0.05	n.m.	3.89 ± 0.03	3.81 ± 0.02	3.90 ± 0.02
Be	0.29 ± 0.08	0.26 ± 0.06	1.72 ± 0.18	n.m.	0.35 ± 0.05	0.33 ± 0.04	0.32 ± 0.03
Pb	1.35 ± 0.04	0.83 ± 0.08	0.55 ± 0.02	n.m.	1.39 ± 0.07	1.17 ± 0.06	0.15 ± 0.06
Bi	0.051 ± 0.009	0.097 ± 0.001	0.108 ± 0.020	n.m.	0.027 ± 0.003	0.049 ± 0.004	0.130 ± 0.009
Mass (mg)	140	140	140		140	140	140

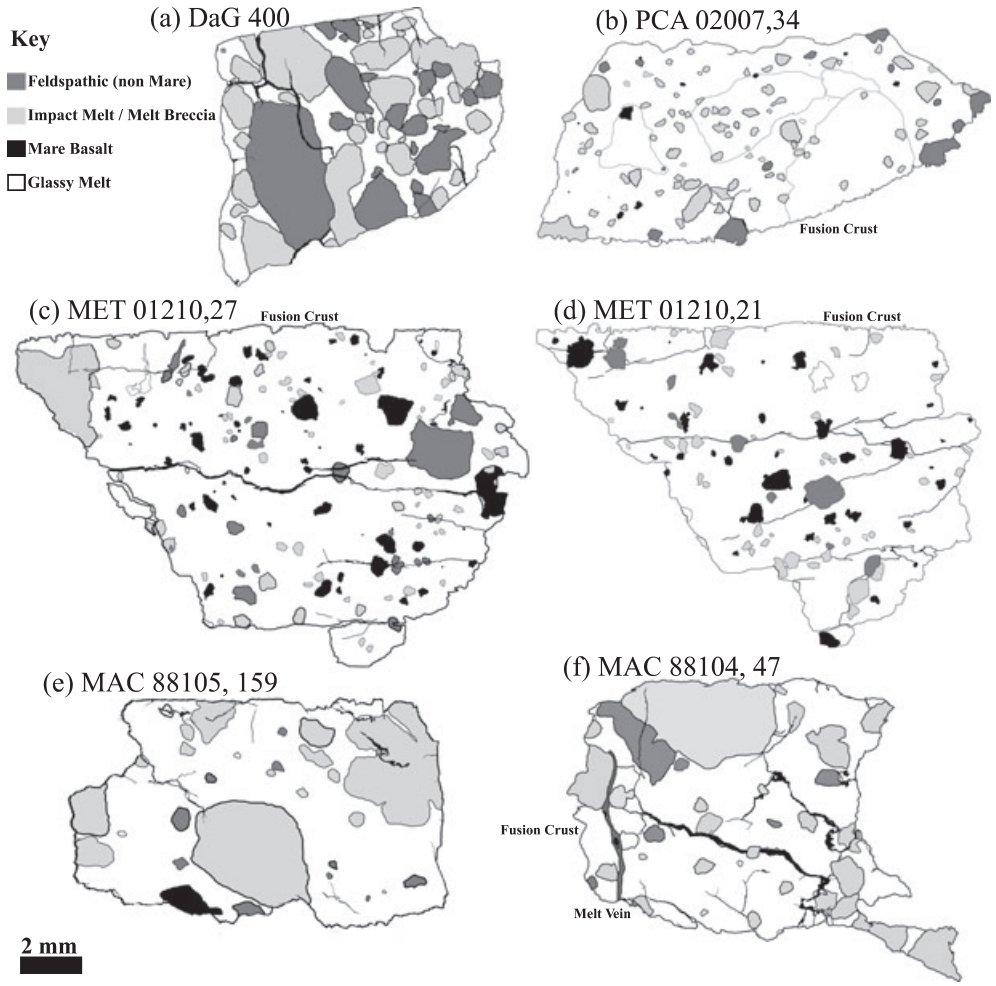

Fig. 1. Classification of clast lithologies within the meteorite samples studied here. Classification derived from texture (Fig. 3), mineral content (Fig. 4), and bulk chemical composition in the meteorite sections (Table 1). a) DaG 400: the largest clast is elongate, has a sub-rounded rim, and is approximately 5 × approximately 2.5 mm. The section is crossed and cut by veins, probably formed through impact melt injection, and some fractures have been infilled with terrestrial $CaCO_3$. b) PCA 02007,34: elongate thin section formed from small clasts (< 1.5 mm) that are mostly derived from impact melt and impact melt breccias. Dashed outlines represent four regolith breccia clasts comprising of a similar range of material as seen in the rest of the sample. c) MET 01210,27 and d) MET 01210,21. Small clasts of mare basalt, impact melt, feldspathic granulites, and monomict mineral fragments are consolidated in a glassy matrix. The sections are cross-cut with variable sized fractures that have a preferred orientation (left to right as shown here). e) MAC 88105,159 and f) MAC 88105,47; large impact melt clasts and ferroan anorthosite clasts are consolidated into a glassy matrix; samples are cross-cut by large fractures that are not infilled with terrestrial contaminants. Scale bar applicable for all images is 2 mm.

MnO is sometimes >80%. Where the relative standard deviation was >100% we removed the value from the reported bulk clast composition.

We acknowledge that there are problems associated with the raster beam analysis technique (i.e., the possible overestimation of elements concentrated in the less-dense phases, and underestimation of elements concentrated in the denser phases, phase edge effects and data acquired from sample cracks and other non-planar surfaces: Albee et al. 1977; Warren 1997; Lindstrom 1999) so, we have corrected the data set using the methodology described by Warren (1997) to account for unequal host phase density effects. This correction method has also been used by Arai and Warren (1999) and by Cohen et al. (2004) and Warren et al. (2005) to report the approximate bulk compositions of impact melt assemblages in QUE 94281 and Dhofar 026, respectively. The corrected RBA clast bulk compositions are shown in Table S1.

Trace Elements

We measured the concentration of minor and trace elements in individual clasts by time-resolved analysis LA-ICP-MS (laser ablation inductively coupled plasma

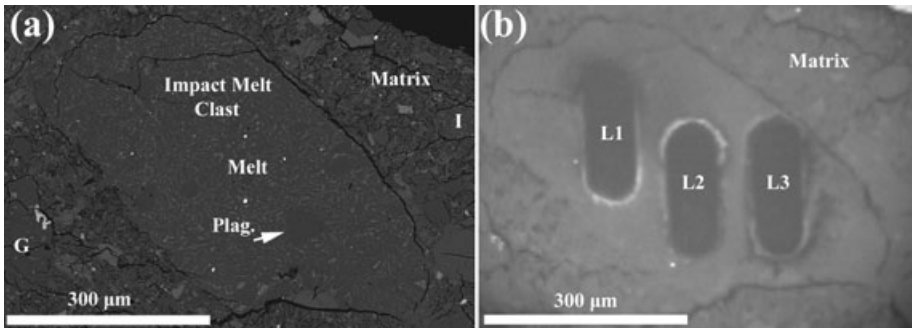

Fig. 2. Impact melt clast in PCA 02007. a) Backscatter electron image before laser ablation analysis showing heterogeneous texture of plagioclase grains included in a matrix of plagioclase and mafic melt. b) Reflected light image of the same clast after trace element investigation by LA-ICP-MS, clearly showing laser tracks of ablated material. Scale bar is 300 μm in both images. L1, L2 and L3 illustrate the three laser ablation pits made in this clast. G = granulized clast, I = impact melt clast, Plag = relict plagioclase clast.

mass spectrometer) at UCL/Birkbeck with a similar instrumental setup to that described in Joy et al. (2008). We utilized a *New Wave* 213 aperture imaged frequency quintupled Nd:YAG laser ablation system (213 nm) coupled to an *Agilent* 7500a quadrupole-based ICP-MS with a shield torch to reduce polyatomic interferences. We operated the laser source with a pulse frequency of 10 to 20 Hz set at 50 to 60% efficiency (conditions dependent on whether the sample was a thick thin section or a block). Data were collected for 55 s, during which time the abundances of 35 to 38 elements was monitored by repeatedly sweeping the mass spectrometer over the intended mass range. Instrumental background levels were established by a "gas blank"; that is, analysis of the mixed He optional gas and Ar carrier gas with the laser off for 30 s. We then ablated the sample for 25 s. The system was purged with He for 30 s between analyses and we waited for at least a further 2 min before proceeding to the next analysis. Data were reduced using the GEMOC Glitter software programme (http://www.glitter-gemoc.com/) where plots of counts per second versus time were examined for each element per analysis, and integration intervals for the gas background and the sample analysis were selected manually. There is a potential risk that in 3-dimensions the laser can penetrate to underlying clast/mineral phases or the glass slide mount, however, this problem is overcome by careful monitoring and selection of the time-resolved signal. Calcium (^{43}Ca) was used as an internal standard, using CaO abundance in clasts by EMP/RBA (Table S1). Analyses were calibrated with NIST 612 external standard measurements (a synthetic doped glass: Pearce et al. 1997) of the same size dimensions. Repeatability of the NIST 612 standard measurements has a total relative standard deviation range of between 1 and 12% for all elements analysed and was typically between 2 and 5%. Accuracy was assessed by comparing our repeat NIST 612 measurements to the Pearce et al. (1997) NIST 612 values, where the relative error was $<4.5\%$ and typically $<2\%$ (i.e., <0.75 ppm absolute error).

The LA-ICP-MS methodology, whilst typically used to measure minor and trace element concentrations in individual mineral (Joy et al. 2006b, 2008; Schnare et al. 2008; Haloda et al. 2009) and glass phases (Norman et al. 1998; Neal and Kramer 2006), also provides an opportunity to measure the bulk composition of polymineralic clasts, multiphase matrix and mesostasis components within small samples mounted into polished thick thin-sections or thick section blocks (Consolmagno et al. 2004; Bland et al. 2005; Joy et al. 2008). Although partially destructive in nature, the technique does not require the whole sample to be disaggregated, ensuring that any untargeted phases in the sample can be studied in the future. Analyses of clast trace element concentrations were performed in situ. Ablated sample material was removed in either several elongated tracks (100–200 μm long) or circular pits depending on the clast size (Fig. 2). Track and circular pit width was 55–80 μm. Ablated masses were removed from different portions of the same clast (within the area previously studied by EMP RBA techniques), to provide a representative study of the clast's bulk composition rather than just the composition of a limited spatial area (i.e., see Fig. 2). Results for each track were averaged together and the errors listed in Table S1 represent the two standard deviation variation of all data collected within a single clast, and do not represent analytical errors. Thus, clasts with large element errors represent rocks that were more mineralogically heterogeneous or coarsely grained (i.e., one measurement may be rather unrepresentative of the total clast composition,

increasing the elemental variability measured by this study), and smaller errors indicate finer grained (i.e., all phases were easily sampled) or more homogenous material. These standard deviations are typically much greater than analytical errors (see above for the range of system precision and accuracy).

We note that TiO_2, MnO, and Cr_2O_3 were measured by both the RBA technique and the LA-ICP-MS technique (Tables 2 and S1). These three elements generally occur at low levels (<1.2 wt% and typically <0.5 wt%) close or below to the detection limit of the EDS detection system (see above). For this reason we have more confidence in the LA-ICP-MS values for these elements and have used these for scientific interpretation.

METEORITE PETROGRAPHY AND IMPACT MELT GEOCHEMISTRY RESULTS

Dar al Gani 400

Dar al Gani (DaG) 400 is a feldspathic polymict regolith breccia lunar meteorite (Zipfel et al. 1998). There have been suggestions (e.g., Korotev et al. 2003; Warren et al. 2005) that the sample is an impact melt breccia (Bukovanska et al. 1999), because the majority of its constituent rock fragments have an impact melt origin (Cohen et al. 2004, 2005; Warren et al. 2005). However, based on the presence of crystalline lithic clasts, large relict mineral fragments and impact melt spherules (Zipfel et al. 1998; Warren et al. 2005), the rock is similar to regolith breccias returned by Apollo missions (McKay et al. 1976, 1986; Simonds et al. 1977; Korotev 1996). Our investigation of DaG 400 did not find any spherules or remnants of a fused soil component. About half of our section consists of clast fragments >500 μm in size (Fig. 1a). This large grain size is proportionally higher than that of material in the Apollo 16 breccias studied by McKay et al. (1986) and is evidence that DaG 400 represents material derived from a comparatively more immature burial environment.

DaG 400 comprises a mixture of lithic and mineral fragments (Fig. 1a) that are fused in a glassy pale gray matrix. Two predominant types of rock fragments occur in DaG 400 (1) clasts that formed as a result of impact melting processes and (2) lithic clasts that crystallized in a non-impact igneous process, which have then been subsequently altered by secondary thermal processes (either shock or regional metamorphism causing granulisation, annealed grain boundaries or shock deformation textures). These igneous lithic clasts have mineral compositions (Fig. 4) indicative of originating from ferroan anorthosite (according to the classification scheme of James et al. [1989] and Floss et al. [1998]) and more magnesian anorthosite bedrock environments.

Impact clasts contribute to approximately 40% of the DaG 400 section. Of these, most are identified as microporphyritic crystalline impact melt breccias containing a clast component (dominantly of plagioclase with minor olivine) formed from either disaggregated grains or grains that have a rounded/sub-rounded grain boundary as a result of resorption into the impact melt (Simonds et al. 1973; Powell et al. 1975). These clasts (Figs. 3a and 3b, see also Cohen et al. 1999) are bound by an amorphous mafic melt matrix. Impact melt with a crystalline texture is rare in our section (Fig. 3c), although has been reported in other DaG 400 studies (Cohen et al. 1999; Warren 2005). Regardless of texture, all of the impact melt and breccia clasts in DaG 400 have bulk major element compositions that can be classified as feldspathic (with 26–31 wt% Al_2O_3; Fig. 5 Table S1) consistent with normative gabbroic/noritic/troctolitic anorthosite. These clasts are within the compositional range of the feldspathic lunar meteorites (Fig. 6) and have a limited range of bulk Mg# compositions ($Mg\#_{63\text{-}67}$: Table S1).

Cold desert feldspathic lunar meteorites typically have bulk CaO/Al_2O_3 ratios of <0.6 (see data compiled by Kevin Righter's "Lunar Meteorite Compendium" and references cited therein). In comparison, hot desert feldspathic lunar meteorites often have a contribution of terrestrially deposited $CaCO_3$ mineralisation causing higher CaO/Al_2O_3 ratios (e.g., >0.6). Six clasts in DaG 400 (Feldspathic 1-3, 5, 7-8: Table S1) appear have CaO/Al_2O_3 ratios of <0.6, suggesting little or no terrestrial contamination. The other six impact clasts (clasts Feldspathic 4, 6, 9-12: Table S1) have CaO/Al_2O_3 ratios of >0.6 indicating excess CaO contents (in this case >17.8 wt%) caused by terrestrially mineralisation. However, we note that all of the DaG 400 clast trace element data (Table S1) indicates that some terrestrially deposited material has been analysed during the laser ablation analysis as Ba and Sr concentrations (>144 and >339 ppm respectively) are too high to be solely indigenous lunar feldspathic impact material (e.g., Apollo 16 low-ITE impact melts groups have <79 ppm Ba and <201 ppm Sr: Korotev 1994). Despite this issue, we do not observe any Ce-anomalies (where Ce/Ce* is defined as the Ce chondrite normalized value, divided by the interpolated value obtained from La and Pr chondrite normalized abundances, and where anomalous data have values outside of >1.5 or <0.75: Crozaz et al. 2003) or LREE-enrichment caused by terrestrial REE mobilization. Crozaz et al. (2003) state that; "As far as the REE are concerned, the whole rock patterns are usually not significantly modified..." by terrestrial contamination

Table 2. Average compositions of the main groups of impact melt in DaG 400, PCA 02007, MET 01210, and MAC 88104/05. Averages derived from data presented in Table S1 based on the clast classification described in the column labeled "compositional sub-type." The column labeled "# of clasts analysed" indicates how many clasts were averaged together to derive a bulk group composition. [a]Average of DaG type 2 feldspathic clasts CaO average taken only from clasts with "low" levels of terrestrial contamination (feldspathic clasts with < 0.6 CaO/Al_2O_3). Errors for group where only one clast is defined as the group (i.e., DaG type 1 and 3, PCA type 1 and 5, and MAC type 3 and 4) are based on the errors for that clast shown in Table S1 (e.g., degree of compositional heterogeneity). Errors for groups where several clast compositions have been averaged together (DaG type 2, MET 1 and 2, PCA type 2, 3, and 4, and MAC type 1, 2, and 5) are based on the 1 standard deviation variation of the individual clast compositions and thus also reflect compositional heterogeneity.
Part 1:

Sample	Impact melt group	Norm. mineralogy	SiO_2	TiO_2	Al_2O_3	FeO	Cr_2O_3	MnO	MgO	CaO	Na_2O	K_2O
DaG 400	DaG Feldspathic type 1	N Anorthosite	45	0.17	29	4.5	b.d.	b.d.	4.3	17.3	0.3	b.d.
DaG 400	DaG Feldspathic type 2 (Average)	T Anorthosite	43	0.24	28	5.0	0.11	0.10	5.4	17.0[a]	0.4	0.05
DaG 400	DaG Feldspathic type 3	T Anorthosite	44	0.33	28	5.2	b.d.	b.d.	5.7	16.7	0.5	0.11
MET 01210	MET Feldspathic type 1 (Average)	N Anorthosite	45	0.29	27	6.5	0.15	0.11	5.9	16.2	0.3	0.04
MET 01210	MET Intermediate Mafic type 2 (Average)	Anorthositic N	45	0.50	24	9.4	0.16	0.14	6.5	14.9	0.3	0.06
PCA 02007	PCA Feldspathic type 1	Anorthosite	44	0.27	32	2.6	b.d.	b.d.	1.8	18.4	0.3	b.d.
PCA 02007	PCA Feldspathic type 2 (Average)	N Anorthosite	45	0.28	28	5.6	0.12	0.06	5.8	16.2	0.4	b.d.
PCA 02007	PCA Mafic type 3 (Average)	Anorthositic N	46	0.26	23	8.9	0.09	b.d.	8.2	14.2	0.2	b.d.
PCA 02007	PCA Mafic type 4 (Average)	Norite	48	0.55	16	15.0	0.40	0.16	9.2	11.2	0.3	b.d.
PCA 02007	PCA Mafic type 5	Norite	47	0.64	13	16.8	0.52	0.22	11.5	10.6	0.3	0.09
MAC 88104/05	MAC Feldspathic type 1 (Average)	N Anorthosite	45	0.12	30	4.7	b.d.	b.d.	3.5	17.4	0.3	b.d.
MAC 88104/05	MAC Feldspathic type 2 (Average)	N Anorthosite	45	0.22	29	5.1	0.07	0.06	4.0	17.0	0.3	b.d.
MAC 88104/05	MAC Feldspathic type 3	N Anorthosite	44	b.d.	28	6.0	b.d.	b.d.	6.4	15.9	0.4	b.d.
MAC 88104/05	MAC High-ITE type 4	N Anorthosite	44	1.15	27	6.6	0.10	b.d.	6.0	15.6	0.5	0.03
MAC 88104/05	MAC Mafic type 5 (Average)	Anorthositic N	47	0.76	18	12.9	0.38	0.12	8.3	12.3	0.5	b.d.
Apollo 16 group 3 Feldspathic Impact Melt Breccias (Korotev 1994)		Anorthosite	45.5	0.34	28.7	4.24	0.09	0.06	4.46	16.1	0.49	0.08
Apollo 16 group 4 Feldspathic Impact Melt Breccias (Korotev 1994)		N Anorthosite	44.7	0.36	31.1	2.91	0.03	0.04	2.80	17.2	0.53	0.05

Part 2:

Sample	Co	Ni	Cu	Zn	Ga	Rb	Sr	Y
DaG 400 type 1	n.m.	n.m.	n.m.	*8 ± 6*	5.4 ± 0.8	0.68 ± 0.05	*323 ± 102*	4.3 ± 0.8
DaG 400 type 2	n.m.	n.m.	n.m.	*7 ± 2*	5.8 ± 1.6	0.78 ± 0.11	*609 ± 57*	7.3 ± 1.3
DaG 400 type 3	n.m.	n.m.	n.m.	*8 ± 1*	3.9 ± 0.6	1.54 ± 0.08	*593 ± 17*	12.8 ± 2.3
MET 01210 type 1	n.m.	n.m.	n.m.	11 ± 6	2.8 ± 0.6	0.97 ± 0.43	146 ± 5	11.1 ± 3.5
MET 01210 type 2	n.m.	n.m.	n.m.	19 ± 5	3.2 ± 0.7	1.54 ± 1.02	132 ± 20	15.7 ± 3.2
PCA 02007 type 1	5.2 ± 1.3	56 ± 33	b.d.	3 ± 1	3.0 ± 0.4	0.31 ± 0.08	149 ± 6	3.3 ± 0.6
PCA 02007 type 2	15.6 ± 1.9	177 ± 58	2.5 ± 0.3	12 ± 3	2.1 ± 0.1	0.36 ± 0.04	149 ± 3	8.6 ± 1.2
PCA 02007 type 3	19.2 ± 0.1	58 ± 16	3.2 ± 0.7	8 ± 1	2.8 ± 0.2	0.15 ± 0.01	113 ± 10	6.4 ± 0.8
PCA 02007 type 4	30.4 ± 11.6	20 ± 3	1.7 ± 0.1	10 ± 4	3.3 ± 0.7	0.27 ± 0.05	107 ± 39	11.2 ± 0.4
PCA 02007 type 5	31.0 ± 1.9	39 ± 8	b.d.	16 ± 16	0.9 ± 0.1	0.59 ± 0.04	55 ± 3	13.7 ± 0.1

Total	Mg#	# clasts	Sc	Ti	TiO_2	V	Cr	Cr_2O_3	Mn	MnO
100	63	1	6.6 ± 1.6	888 ± 200	0.15 ± 0.03	15 ± 4	485 ± 224	0.07 ± 0.03	581 ± 390	0.07 ± 0.05
99	66	10	8.7 ± 0.6	1300 ± 112	0.22 ± 0.02	19 ± 2	590 ± 48	0.09 ± 0.01	1011 ± 83	0.13 ± 0.01
100	66	1	7.7 ± 1.2	1408 ± 256	0.23 ± 0.04	19 ± 3	590 ± 91	0.09 ± 0.01	990 ± 156	0.13 ± 0.02
102	62	8	13.0 ± 1.6	2045 ± 574	0.34 ± 0.10	22 ± 4	759 ± 167	0.11 ± 0.02	586 ± 71	0.08 ± 0.01
102	55	9	21.2 ± 6.4	3041 ± 978	0.51 ± 0.16	32 ± 12	977 ± 311	0.14 ± 0.05	784 ± 171	0.10 ± 0.02
100	56	1	6.2 ± 1.0	360 ± 57	0.06 ± 0.01	16 ± 3	318 ± 64	0.05 ± 0.01	230 ± 60	0.03 ± 0.01
101	65	12	10.5 ± 0.4	1524 ± 89	0.25 ± 0.01	21 ± 1	723 ± 24	0.11 ± 0.01	486 ± 20	0.06 ± 0.01
101	62	3	19.2 ± 3.7	1939 ± 397	0.32 ± 0.07	54 ± 15	1403 ± 351	0.21 ± 0.05	845 ± 110	0.11 ± 0.01
101	52	4	54.5 ± 15.3	3987 ± 411	0.67 ± 0.07	177 ± 70	3614 ± 649	0.53 ± 0.09	2864 ± 103	0.37 ± 0.01
100	55	1	50.7 ± 1.7	3508 ± 136	0.59 ± 0.02	130 ± 3	3492 ± 174	0.51 ± 0.03	1672 ± 28	0.22 ± 0.01
100	57	2	10.3 ± 0.8	1417 ± 92	0.24 ± 0.02	15 ± 1	487 ± 46	0.07 ± 0.01	677 ± 35	0.09 ± 0.01
101	59	9	12.3 ± 2.2	1865 ± 170	0.31 ± 0.03	21 ± 4	684 ± 150	0.10 ± 0.02	728 ± 83	0.09 ± 0.01
101	66	1	12.1 ± 3.6	1022 ± 852	0.17 ± 0.14	33 ± 12	1188 ± 412	0.17 ± 0.06	1440 ± 1116	0.19 ± 0.14
101	62	1	16.3 ± 0.1	15222 ± 996	2.54 ± 0.17	28 ± 3	935 ± 164	0.14 ± 0.02	916 ± 31	0.12 ± 0.01
101	54	3	36.5 ± 3.7	7339 ± 3155	1.22 ± 0.53	87 ± 2	2052 ± 99	0.30 ± 0.01	1770 ± 25	0.23 ± 0.01
100	65		7.9		0.34		650	0.10		
100	62		5.4		0.36		360	0.05		0.04

Zr	Nb	Cs	Ba	La	Ce	Pr	Nd	Sm
14 ± 2	1.3 ± 0.2	0.04 ± 0.01	127 ± 20	1.32 ± 0.18	3.64 ± 0.55	0.49 ± 0.07	2.06 ± 0.24	0.60 ± 0.11
26 ± 5	1.9 ± 0.3	0.04 ± 0.06	372 ± 195	2.16 ± 0.40	5.79 ± 1.02	0.76 ± 0.13	3.55 ± 0.63	1.01 ± 0.16
52 ± 9	3.8 ± 0.5	0.06 ± 0.05	248 ± 55	4.14 ± 0.71	10.97 ± 1.78	1.47 ± 0.27	6.49 ± 1.19	1.74 ± 0.36
39 ± 11	2.7 ± 1.2	0.40 ± 0.79	40 ± 16	3.00 ± 1.14	7.42 ± 2.90	0.96 ± 0.36	4.86 ± 1.71	1.36 ± 0.59
56 ± 19	3.7 ± 1.4	0.34 ± 0.71	54 ± 19	3.99 ± 1.19	9.24 ± 2.77	1.31 ± 0.34	6.27 ± 1.69	1.90 ± 0.67
10 ± 1	0.7 ± 0.1	0.03	11 ± 1	1.04 ± 0.27	3.17 ± 0.88	0.47 ± 0.09	1.86 ± 0.31	0.44 ± 0.10
29 ± 8	1.9 ± 0.3	0.03 ± 0.01	25 ± 2	2.08 ± 0.36	5.07 ± 0.77	0.72 ± 0.10	3.51 ± 0.51	1.01 ± 0.23
13 ± 1	0.7 ± 0.1	0.02	14 ± 0	0.88 ± 0.08	2.23 ± 0.21	0.31 ± 0.01	1.63 ± 0.05	0.57 ± 0.01
20 ± 5	1.3 ± 0.6	0.03	20 ± 4	1.17 ± 0.37	3.48 ± 0.63	0.42 ± 0.08	2.33 ± 0.77	0.80 ± 0.03
35 ± 1	2.5 ± 0.2	0.03 ± 0.01	36 ± 1	2.49 ± 0.10	6.11 ± 0.30	0.84 ± 0.06	4.10 ± 0.18	1.41 ± 0.02

Table 2. *Continued*. Average compositions of the main groups of impact melt in DaG 400, PCA 02007, MET 01210, and MAC 88104/05. Averages derived from data presented in Table S1 based on the clast classification described in the column labeled "compositional sub-type." The column labeled "# of clasts analysed" indicates how many clasts were averaged together to derive a bulk group composition. [a]Average of DaG type 2 feldspathic clasts CaO average taken only from clasts with "low" levels of terrestrial contamination (feldspathic clasts with < 0.6 CaO/Al_2O_3). Errors for group where only one clast is defined as the group (i.e., DaG type 1 and 3, PCA type 1 and 5, and MAC type 3 and 4) are based on the errors for that clast shown in Table S1 (e.g., degree of compositional heterogeneity). Errors for groups where several clast compositions have been averaged together (DaG type 2, MET 1 and 2, PCA type 2, 3, and 4, and MAC type 1, 2, and 5) are based on the 1 standard deviation variation of the individual clast compositions and thus also reflect compositional heterogeneity.

Sample	Co	Ni	Cu	Zn	Ga	Rb	Sr	Y
MAC 88104/05 type 1	8.9 ± 0.1	26 ± 10	2.6 ± 0.9	5 ± 1	3.0 ± 0.2	0.63 ± 0.21	142 ± 1	4.2 ± 0.4
MAC 88104/05 type 2	14.3 ± 1.1	142 ± 51	3.2 ± 0.5	4 ± 1	3.4 ± 0.5	0.69 ± 0.12	148 ± 3	9.5 ± 1.0
MAC 88104/05 type 3	25.0 ± 25.3	80 ± 60	2.3 ± 0.03	34 ± 42	3.4 ± 0.1	0.97 ± 0.55	148 ± 2	5.5 ± 3.7
MAC 88104/05 type 4	19.0 ± 1.9	130 ± 8	3.4 ± 0.2	9 ± 6	6.2 ± 0.1	1.76 ± 0.13	183 ± 1	95.5 ± 3.8
MAC 88104/05 type 5	24.0 ± 3.1	96 ± 43	2.7 ± 0.8	6 ± 2	3.0 ± 0.5	0.83 ± 0.29	96 ± 5	19.3 ± 7.6
Apollo 16 group 3	16.9	190				2.20	178	
Apollo 16 group 4	6.90	43				0.90	192	

Part 3:

Sample	Eu	Gd	Tb	Dy	Ho	Er	Tm
DaG 400 type 1	0.72 ± 0.04	0.67 ± 0.10	0.11 ± 0.02	0.84 ± 0.12	0.18 ± 0.05	0.50 ± 0.11	0.07 ± 0.01
DaG 400 type 2	0.81 ± 0.05	1.18 ± 0.23	0.20 ± 0.03	1.43 ± 0.23	0.30 ± 0.04	0.87 ± 0.13	0.13 ± 0.02
DaG 400 type 3	0.75 ± 0.12	2.06 ± 0.44	0.34 ± 0.06	2.42 ± 0.38	0.49 ± 0.09	1.44 ± 0.25	0.20 ± 0.05
MET 01210 type 1	0.75 ± 0.05	1.74 ± 0.57	0.31 ± 0.09	2.04 ± 0.68	0.45 ± 0.16	1.28 ± 0.33	0.20 ± 0.05
MET 01210 type 2	0.84 ± 0.17	2.40 ± 0.58	0.42 ± 0.09	3.04 ± 0.73	0.61 ± 0.14	1.68 ± 0.43	0.28 ± 0.06
PCA 02007 type 1	0.69 ± 0.09	0.40 ± 0.21	0.10 ± 0.05	0.64 ± 0.16	0.13 ± 0.03	0.36 ± 0.09	0.05 ± 0.03
PCA 02007 type 2	0.84 ± 0.02	1.25 ± 0.15	0.23 ± 0.04	1.52 ± 0.20	0.34 ± 0.05	0.97 ± 0.10	0.13 ± 0.03
PCA 02007 type 3	0.67 ± 0.21	0.61 ± 0.10	0.16 ± 0.04	1.17 ± 0.23	0.26 ± 0.03	0.84 ± 0.21	0.11 ± 0.04
PCA 02007 type 4	0.66 ± 0.14	1.16 ± 0.27	0.24 ± 0.02	2.00 ± 0.05	0.46 ± 0.09	1.44 ± 0.05	0.23 ± 0.01
PCA 02007 type 5	0.37 ± 0.04	1.70 ± 0.28	0.31 ± 0.01	2.48 ± 0.07	0.54 ± 0.06	1.69 ± 0.13	0.28 ± 0.01
MAC 88104/05 type 1	0.73 ± 0.04	0.54 ± 0.07	0.13 ± 0.00	0.73 ± 0.10	0.19 ± 0.02	0.48 ± 0.02	0.09 ± 0.01
MAC 88104/05 type 2	0.84 ± 0.04	1.41 ± 0.13	0.27 ± 0.02	1.77 ± 0.16	0.38 ± 0.04	1.06 ± 0.10	0.16 ± 0.02
MAC 88104/05 type 3	0.82 ± 0.11	0.79 ± 0.52	0.17 ± 0.08	1.08 ± 0.76	0.23 ± 0.16	0.68 ± 0.33	0.14 ± 0.08
MAC 88104/05 type 4	2.00 ± 0.02	19.59 ± 0.86	3.07 ± 0.12	20.65 ± 1.03	3.93 ± 0.11	10.58 ± 0.35	1.46 ± 0.01
MAC 88104/05 type 5	0.74 ± 0.08	2.92 ± 1.16	0.50 ± 0.18	3.60 ± 1.36	0.75 ± 0.27	2.19 ± 0.82	0.33 ± 0.13
Apollo 16 group 3	1.06		0.65				
Apollo 16 group 4	1.14		0.23				

"...and valuable petrogenetic information can still be retrieved"; therefore we are confident that the elemental abundances measured in DaG 400 impact melt data (excluding Ca, Sr, Ba, and possibly U) are reliably indicative of original lunar chemistry.

Our study (Table S1) shows that all impact material in DaG 400 can be classified as ITE-poor (< 2 ppm Sm: Figs. 6e and 6f), feldspathic impact-melt (following the criteria of McKinley et al. 1984 and Korotev 1994 based on studies of impact melt rocks from the Apollo 16 site). All the clasts are relatively LREE-rich (La_{cn}/Lu_{cn} 1.5 to 2.2 where $_{cn}$ refers to chondrite normalizing values of Anders and Grevesse 1989), have small Eu-anomalies (Eu/Eu* 1.2 to 3.5, where $Eu/Eu^* = Eu_{cn}/\sqrt{[Sm_{cn} \times Gd_{cn}]}$), and flat HREE patterns (Fig. 7a). Most clasts fall into a single group (which we term the DaG type 2 group: Tables 2 and S1) that have $\times 4_{cn}$ to $\times 14_{cn}$ (for trivalent REE). We also observe two other compositional types of impact melt breccia clast where one fragment (DaG type 3: Table 2) is troctolitic anorthosite normative with slightly higher REE abundances ($\times 8_{cn}$ to $\times 18_{cn}$ for trivalent REE elements) and a second clast (DaG type 1: Table 2) is gabbroic/noritic anorthosite normative and has slightly lower concentrations ($\times 3_{cn}$ to $\times 6_{cn}$ for trivalent REE elements) than the DaG type 2 feldspathic impact melt main group.

Meteorite Hills 01210

This meteorite was originally classified as being a basaltic bearing anorthositic breccia (Russell et al. 2004), but in fact the meteorite is an anorthosite bearing basaltic lunar regolith breccia (Day et al. 2006; Terada

Zr	Nb	Cs	Ba	La	Ce	Pr	Nd	Sm
12 ± 0	1.0 ± 0.0	n.m.	13 ± 1	0.87 ± 0.07	2.12 ± 0.01	0.41 ± 0.03	1.54 ± 0.01	0.52 ± 0.05
32 ± 4	2.5 ± 0.3	n.m.	31 ± 3	2.56 ± 0.24	6.07 ± 0.69	0.97 ± 0.09	4.24 ± 0.34	1.26 ± 0.16
12 ± 13	0.7 ± 0.6	n.m.	20 ± 11	1.18 ± 0.29	2.37 ± 1.36	0.47 ± 0.09	1.97 ± 0.74	0.64 ± 0.34
460 ± 30	24.6 ± 0.7	n.m.	191 ± 9	34.37 ± 1.39	87.31 ± 3.24	13.13 ± 0.25	62.27 ± 1.65	17.50 ± 0.52
64 ± 26	4.6 ± 1.8	n.m.	48 ± 14	4.54 ± 1.56	11.08 ± 3.21	1.70 ± 0.49	7.90 ± 2.72	2.40 ± 0.77
100		0.09	79	6.99	18.20		11.00	3.19
35		0.04	42	2.37	6.10		3.90	1.12

Yb	Lu	Hf	Ta	W	Pb	Th	U	# clasts
0.53 ± 0.12	0.07 ± 0.02	0.34 ± 0.05	0.06 ± 0.01	0.07 ± 0.05	0.15 ± 0.04	0.18 ± 0.01	0.09 ± 0.03	1
0.86 ± 0.13	0.12 ± 0.02	0.69 ± 0.10	0.10 ± 0.02	0.05 ± 0.02	0.37 ± 0.14	0.36 ± 0.08	0.22 ± 0.06	10
1.34 ± 0.26	0.20 ± 0.05	1.24 ± 0.19	0.17 ± 0.04	0.09 ± 0.01	0.39 ± 0.04	0.66 ± 0.11	0.29 ± 0.04	1
1.23 ± 0.35	0.19 ± 0.07	1.06 ± 0.34	0.16 ± 0.06	0.13 ± 0.06	0.37 ± 0.10	0.58 ± 0.22	0.15 ± 0.08	5
1.88 ± 0.28	0.26 ± 0.06	1.43 ± 0.54	0.18 ± 0.08	0.14 ± 0.03	0.72 ± 0.67	0.94 ± 0.65	0.19 ± 0.07	7
0.34 ± 0.13	0.05 ± 0.02	0.18 ± 0.01	0.03 ± 0.01	b.d.	0.11 ± 0.06	0.16 ± 0.03	0.07 ± 0.03	1
0.97 ± 0.13	0.14 ± 0.02	0.77 ± 0.24	0.10 ± 0.01	0.06 ± 0.02	0.16 ± 0.01	0.32 ± 0.08	0.07 ± 0.01	7
0.63 ± 0.15	0.11 ± 0.06	0.46 ± 0.03	0.04 ± 0.01	b.d.	0.13 ± 0.05	0.12 ± 0.04	0.03 ± 0.01	2
1.61 ± 0.12	0.29 ± 0.04	0.73 ± 0.18	0.07 ± 0.06	b.d.	0.20 ± 0.02	0.14 ± 0.04	0.06 ± 0.03	2
1.94 ± 0.33	0.28 ± 0.07	1.18 ± 0.01	0.13 ± 0.01	0.07 ± 0.04	0.16 ± 0.04	0.54 ± 0.12	0.18 ± 0.01	1
0.51 ± 0.04	0.09 ± 0.02	0.29 ± 0.01	0.10 ± 0.01	n.m.	0.27 ± 0.01	0.13 ± 0.01	0.25 ± 0.06	2
1.12 ± 0.12	0.16 ± 0.02	0.81 ± 0.11	0.15 ± 0.02	n.m.	0.38 ± 0.06	0.55 ± 0.29	0.25 ± 0.08	9
0.78 ± 0.38	0.16 ± 0.03	0.42 ± 0.41	0.06 ± 0.06	n.m.	0.33 ± 0.15	0.18 ± 0.19	0.21 ± 0.08	1
9.39 ± 0.52	1.27 ± 0.03	11.61 ± 0.76	1.58 ± 0.10	n.m.	1.17 ± 0.06	3.34 ± 0.14	0.88 ± 0.01	1
2.29 ± 0.81	0.32 ± 0.12	1.61 ± 0.69	0.26 ± 0.11	n.m.	0.39 ± 0.06	0.69 ± 0.21	0.28 ± 0.06	3
2.35	0.33		2.42	0.28		1.16	0.31	
0.91	0.127		0.85	0.12		0.37	0.11	

et al. 2007a; Joy et al. 2008; Korotev et al. 2009). The thin sections studied in this investigation both have vesicular fusion crusts and are samples of an immature polymict regolith. The lithic fragment size is generally small in our sections (Figs. 1c and 1d), with a few clasts being as large as 0.5 cm in size and the majority being $<<1$ mm. MET 01210 is a regolith breccia as it contains a component of small impact melt spherules, rounded glass agglutinates and glassy melt aggregates.

The stone is formed from a dark glassy gray matrix enclosing small white, gray and brown mineral fragments and lithic clasts. These lithic fragments include examples of a texturally distinct range of low-Ti to very low-Ti (VLT) basalts including intergranular subophitic varieties and some with fine-grained feathery plumose textures (Day et al. 2006; Arai et al. 2010). There is also a significant feldspathic highlands component in our sections, including small granulites and recrystallized anorthosites (Day et al. 2006), mafic norite and troctolite clasts (see Fig. 4 for a summary of mineral chemistry variation).

Impact melt and breccias together contribute to approximately 6% (by mode) of the MET 01210,21 and MET 01210,27 sections and are present in about the same proportions as nonimpact mare basalt lithic clast material (Joy 2007). We observe both holocrystalline (Figs. 3e and 3f) impact melt (with intersertal or variolitic textures) and impact melt breccias (Fig. 3d) in the sample. These are similar to those in MET 01210 reported by Day et al. (2006). Compositionally clasts include feldspathic varieties equivalent to normative noritic anorthosite (with >26 wt% Al_2O_3, <15.5 ppm Sc: e.g., MET type 1 listed in Tables 2 and S1), and those with mafic compositions consistent with a

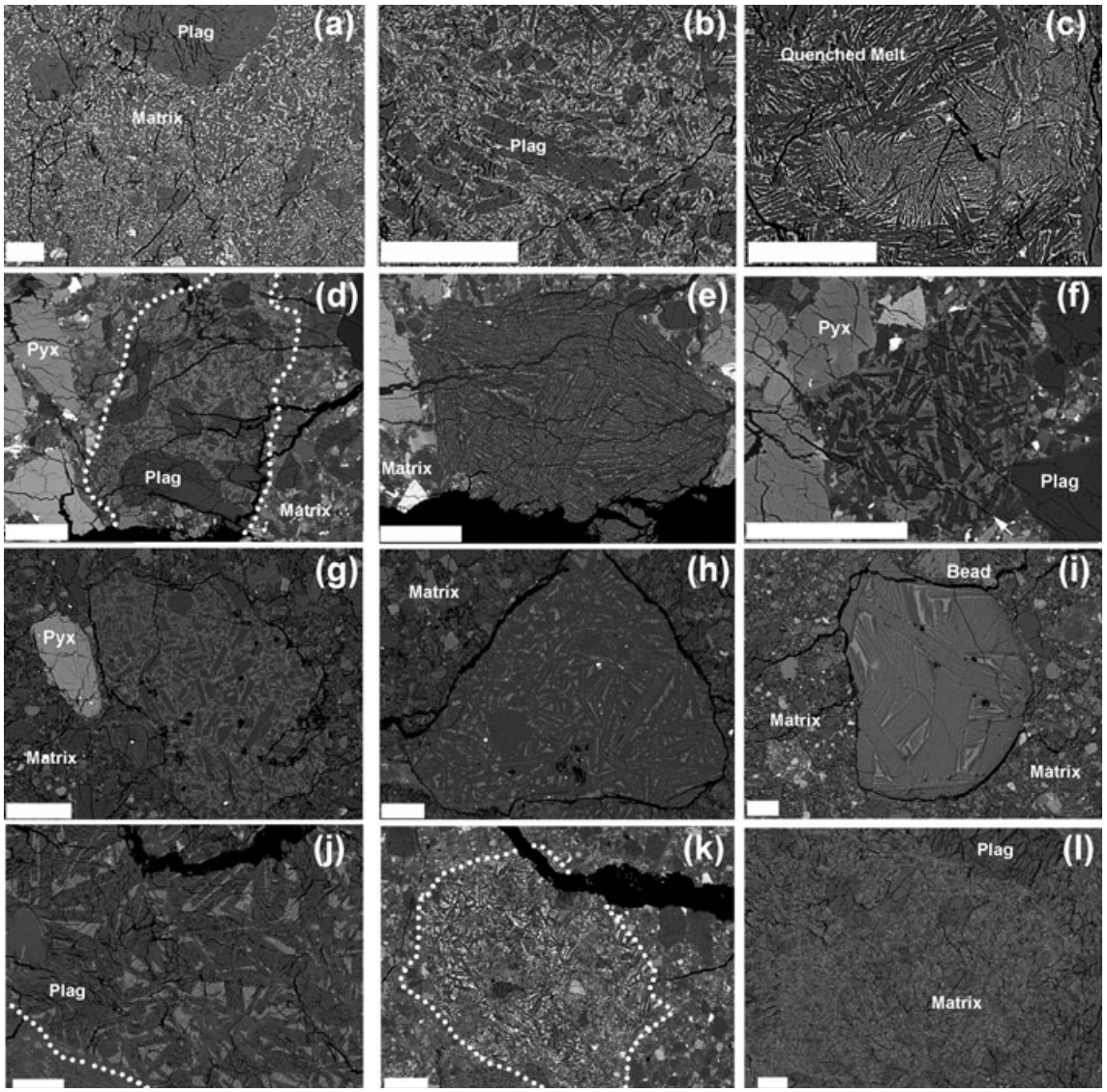

Fig. 3. Backscatter electron (BSE) microscope images of impact melt clasts. DaG 400. a) Clastic melt with large inclusions of plagioclase and minor olivines with rounded grain boundaries from thermal erosion in the melt. b) Clastic melt small clasts of plagioclase in a much finer melt matrix with small plagioclase and crypto-pyroxene melt. c) Non-clastic quenched clast with very small melt crystals radiating from nucleation points. MET 01210. d) Clastic impact melt breccia with different sized inclusions of plagioclase grains. e) Devitrified microcrystalline impact-melt clast. f) Intersertal melt clasts with plagioclase laths ophitically enclosing mafic glassy melt pockets. PCA 02007. g) Non-clastic melt clast with tabular plagioclase laths in a mafic glass melt matrix. h) Large intersertal melt clast with plagioclase laths enclosing mafic glassy melt pockets similar to the ''reannealed feldspathic'' clast shown in figure 8n of Day et al. (2006). i) Large quenched feldspathic impact melt glass fragment. MAC 88104/05. j) and k) Basaltic microcrystalline melt clasts. l) Clastic single generation melt with different size inclusions of plagioclase chadacrysts. Plag = plagioclase, Pyx = pyroxene, Dotted outline denotes clast boundary. Scale bar represents 100 μm.

normative mineralogy of noritic anorthosite to anorthositic norite (19–26 wt% Al_2O_3, >15.5 ppm Sc: e.g., MET type 2 listed in Tables 2 and S1).

Pecora Escarpment 02007

This meteorite is a feldspathic regolith breccia, with a minor basaltic lithic component (Day et al. 2006; Korotev et al. 2006). We observe rare small (< 500 μm) clasts of VLT basalt in section PCA 02007,34 (Fig. 1b) and Day et al. (2006) also report basalt/gabbro clasts in PCA 02007. The stone is classified as a regolith derived breccia as it contains several impact melt spherules, glassy agglutinates, and a rare meteoritic metallic component (Korotev et al. 2006) and a possible chondritic meteorite fragment (Day et al. 2006).

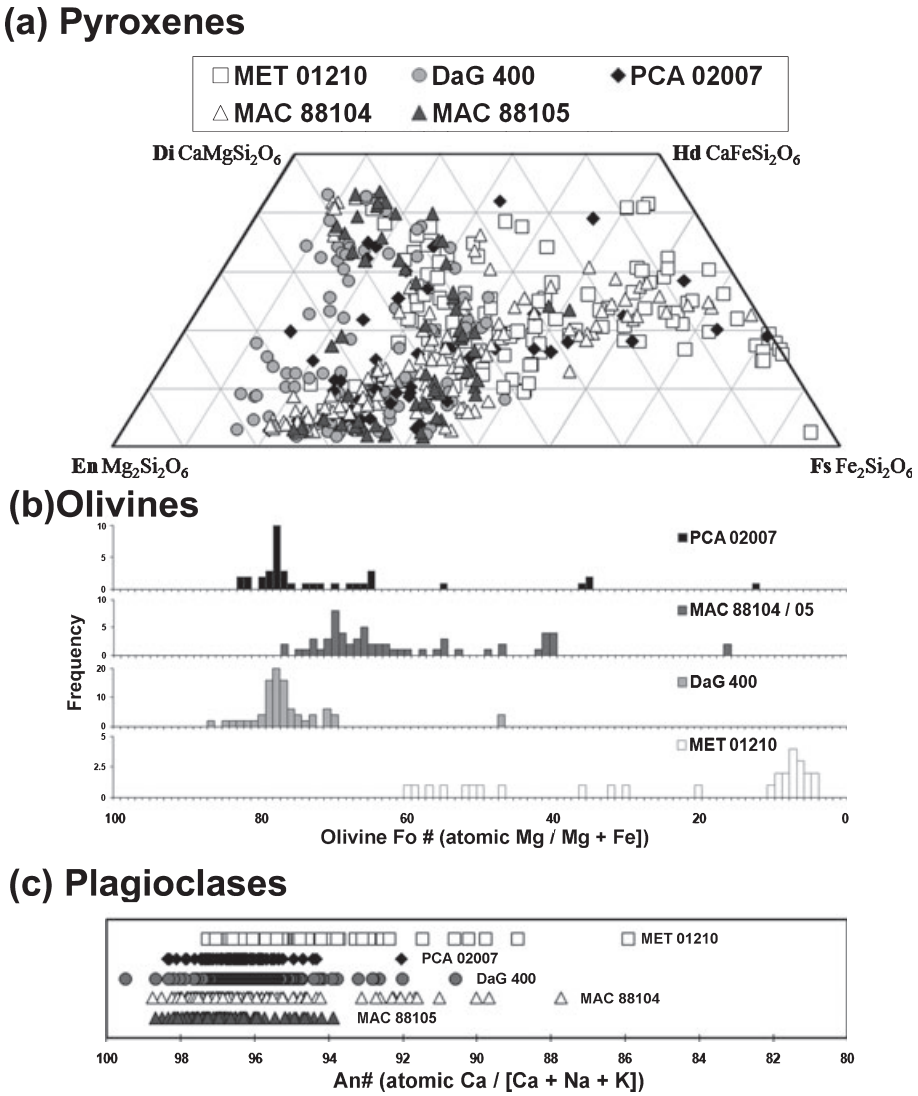

Fig. 4. Mineral compositions of lithic clasts and mineral fragments in DaG 400, MET 01210, and PCA 02007. a) Pyroxene compositions in the meteorite samples. b) Histogram of Fo (forsterite) content of olivine grains. c) Anorthite composition range in the stones.

Our section of PCA 02007 contains a thin, highly vesiculated fusion crust. The sample contains a seriate range of monomict mineral clasts, polymict lithic clasts and glass fragments fused together in a glassy melt and comminuted rock matrix. Lithic and mineral clasts are commonly surrounded by fractures that easily distinguish them from the fine grained matrix (for example Fig. 3h) and suggest that the source regolith was poorly shock welded together. Glassy clast fragments commonly have irregular grain boundaries and some have a highly vesicular texture indicating that they are agglutinatic in origin. The lithic fragment size is the smallest of the three meteorites studied, with all lithic clasts being <1.5 mm in size (Fig. 1b), suggesting that the rock was consolidated in a relatively mature regolith environment (McKay et al. 1976).

Impact melt and breccia clasts exhibit a large range in grain size and form both the smallest material identified in the section (< 20 μm) to the largest clasts (approximately 1.3 mm in length) (see also descriptions by Day et al. 2006 and Korotev et al. 2006). Approximately 20% of all lithic clasts within PCA 02007,34 were impact derived and of this fraction approximately 60% are nonclastic microcrystalline impact melt varieties (Figs. 3h and 3i) and approximately 40% are clastic impact melt breccias (where plagioclase is the dominate clast type).

We observe two types of feldspathic melts in PCA 02007. The first group (PCA type 1: Tables 2 and S1) is characterized by just a single anorthosite normative clast (Fig. 5) with low concentrations of incompatible trace elements ($\times 2_{cn}$ to $\times 6_{cn}$ for trivalent REE). The

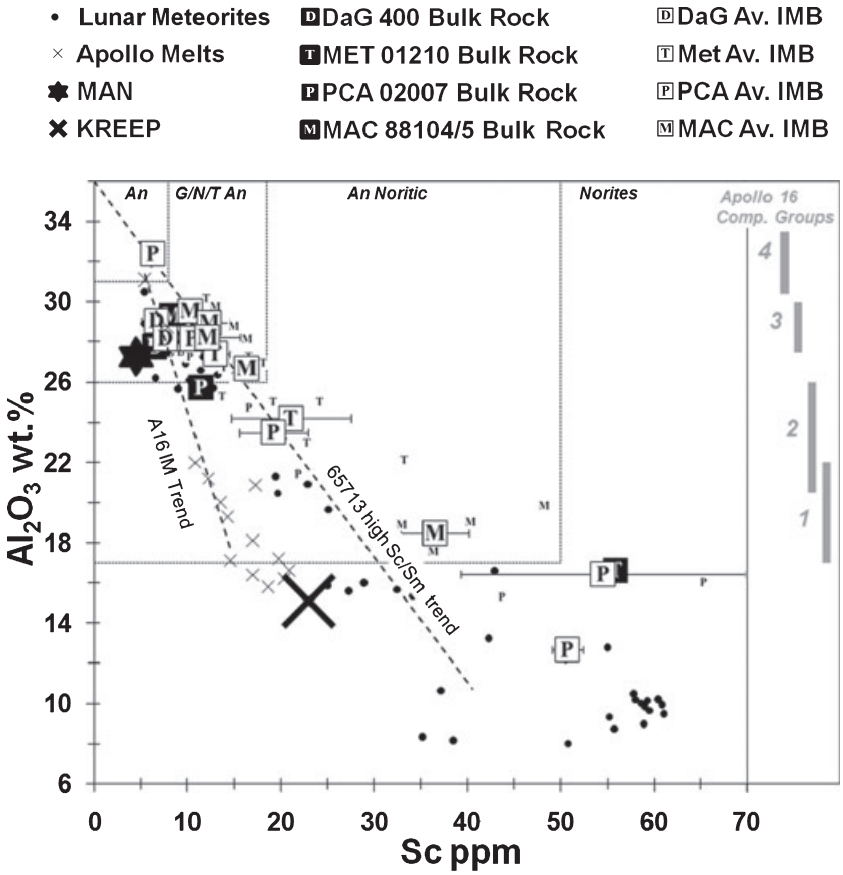

Fig. 5. Bulk Sc versus Al_2O_3 compositions of impact melt and melt breccia clasts in this study (Tables 1, 2, and S1) compared with bulk composition of lunar meteorite samples (taken from range of literature sources including the online supporting material table A3.9 of Wieczorek et al. [2006]; Sokol et al. [2008]; and data compiled by Kevin Righter for the "Lunar Meteorite Compendium" http://curator.jsc.nasa.gov/antmet/lmc/index.cfm) and mean composition of Apollo impact melt groups (mafic groups listed in Jolliff [1998] and feldspathic groups listed in Korotev [1994]). Meteorite bulk sample compositions (Table 1) are shown as large symbols with white text and black background (D = Dag 400, T = MET 01210, P = PCA 02007 and M = MAC 88104/05). Average meteorite impact melt breccia compositional groups (Table 2) are shown as large symbols with black text and white background (Av. IMB). Individual impact melt data points (Table S1) are shown as small versions of the same symbol with black text and white background. Error bars for Sc are 1σ error as listed in Table 2. Al_2O_3 values of individual impact melt clasts (Table S1) and compositional melt groups (Table 2) are "corrected" raster beam analysis values to account for the unequal host-phase density effect described by Warren (1997). The Apollo 16 compositional groups (grey bars at right of image) show the range of the four impact melt compositional groups as listed in Fig. 1 of Korotev (1994). KREEP symbol denotes high-K KREEP concentrations listed by Warren (1989). MAN symbol = Magnesian Anorthosite Suite as defined by the bulk composition of Dhofar 489 lunar meteorite (Korotev et al. 2006). The trend of rock fragments from sample 65713 is taken from Jolliff and Haskin (1995). The Apollo 16 melt trend is a linear fit through the Apollo 16 impact melt group average compositions listed in Korotev (1994) and Jolliff (1998). Normative mineralogies are based on CIPW-norms of impact melt clasts in this study where An = anorthosite normative; G/N/T An = gabbroic/noritic/troctolitic anorthosite normative; An N = anorthositic norite normative; and Norite = norite normative.

other twelve noritic anorthosite normative feldspathic clasts identified in this study we group together into as single type termed PCA type 2 (Tables 2 and S1).

Mafic impact melt clasts (Tables 2 and S1: PCA Mafic Melt 1–7) are characterized by lower Al_2O_3 (< 26 wt%) and higher concentrations of Sc (> 15.5 ppm Sc: Figs. 5 and 6c, 6e) compared with the PCA 02007 feldspathic melts (<12 ppm Sc: Figs. 5 and 6c, 6e). We identify a single norite normative impact melt clast in PCA 02007 (Mafic 7: Table S1) with a basalt-like composition (< 13 wt% Al_2O_3, < 50 ppm Sc, La_{cn}/Lu_{cn} 0.94, and a negative Eu-anomaly; Eu/Eu* 0.67). However, this type of mafic impact melt differs from the Apollo mafic impact melts (Jolliff 1998; Korotev 2000) as it is has lower ITE and Sc concentrations (Figs. 5 and 6c, 6e).

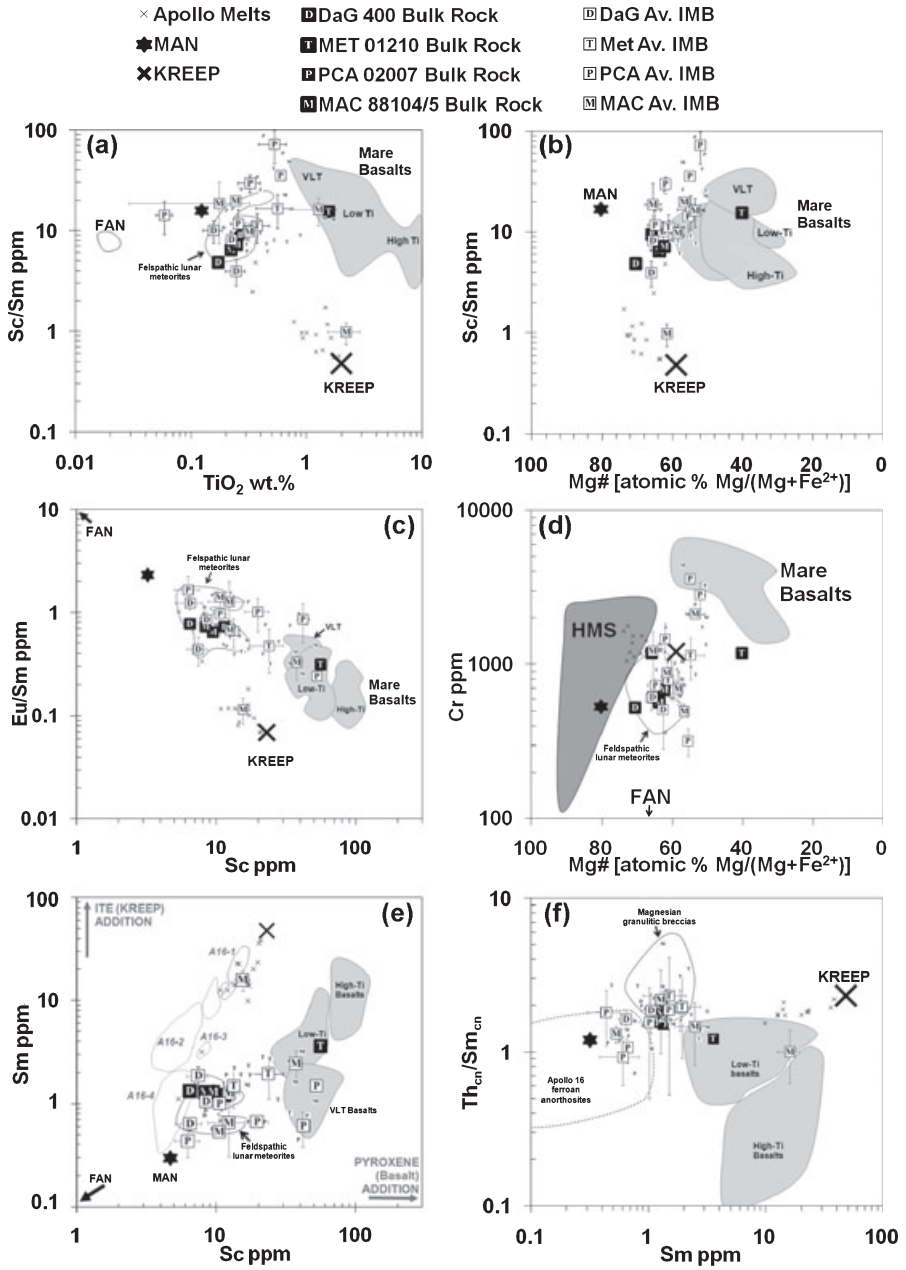

Fig. 6. Bulk compositions of meteorites and impact melt and melt breccia clasts in DaG 400, MET 01210, PCA 02007 and MAC 88104/05 (Tables 2 and S1). Symbols are the same as Fig. 5. Error bars on the composition "groups" are the 1σ error as listed in Table 2 and represent clast compositional heterogeneity. a) Plot of Sc/Sm versus TiO_2 (where TiO_2 is taken from LA-ICP-MS TiO_2 values); b) Sc/Sm versus Mg#; c) Eu/Sm versus Sc (ppm); d) Cr (ppm) versus Mg#; e) Sc versus Sm [n.b. Sc is highly compatible in the pyroxene crystal structure and can be a used a good assessment of how much mafic material has been incorporated into the melt (Jolliff and Haskin 1995). Sm is used as a measure of incompatible trace elements in lunar impact melts (Jolliff and Haskin 1995), where high ITE signatures are typically acquired from KREEP assimilation]. Impact melt clasts compositions in (e) are compared with the rocks identified by McKinley et al. (1984) and Korotev (1994) as group 1 (A16-G1) Apollo 16 "LKFM" varieties and KREEPy basalts; group 2 (A16-G2) VHA basalts, impact-melts splashes and bombs; group 3 (A16-G3) Anorthositic basalts, FAN rocks; group 4 (A16-G4) Feldspathic, fragment laden, melt breccia, intergranular breccias and feldspathic microporphyritic melt breccias.]; f) Sm versus Th_{cn}/Sm_{cn} (where the magnesian granulitic breccias and Apollo 16 ferroan noritic anorthosite fields are taken from figure 16a of Korotev et al. [2003]). Bulk compositions of Apollo and meteorite samples are taken from a variety of references including those listed in Fig. 5 and in BVSP (1981); Taylor et al. (1991); Papike et al. (1998), the "mare basalt database" that is part of the electronic appendix of Jolliff et al. (2006) and the online supporting material table A3.1 to A3.12 of Wieczorek et al. (2006). FAN symbol represents sample 15415 "genesis rock" (Ryder 1985) and 60025 (Haskin et al. 1973). Other sample composition references are as described in Fig. 5.

MacAlpine Hills 88104/88105

The meteorite is classified as an anorthositic polymict regolith breccia with ferroan anorthosite, impact melt and metaclastic granulitic clasts consolidated into a fine-grained glassy melt matrix (Jolliff et al. 1991; Koeberl et al. 1991; Lindstrom et al. 1991; Neal et al. 1991). Our sections are cross-cut by large fractures and MAC 88104,47 contains a fusion crust and large glassy melt vein (Figs. 1e and 1f). Clasts principally comprise feldspathic impact melt breccias, gabbroic anorthosites and noritic anorthosites with rare anorthositic troctolite fragments and basalt clasts. The mineral chemistry of clast and matrix fragments in the samples is shown in Fig. 4. MAC 88104,47 contains a large (2×5 mm) ferroan ($Mg\#_{57}$) cataclastic breccia with fragmented pyroxenes ($En_{1\text{-}74}$, $Fs_{22\text{-}76}$, $Wo_{3\text{-}36}$), plagioclase ($An_{94\text{-}98}$), olivines ($Fo_{40\text{-}57}$), silica, and disseminated troilite grains. We found a small (700×1500 μm) hyperferroan granulite in MAC 88105,159 with pyroxene ($En_{36\text{-}45}$, $Fs_{24\text{-}45}$, $Wo_{11\text{-}40}$), olivine ($Fo_{39\text{-}41}$), plagioclase ($An_{94\text{-}97}$), and small grains of ilmenite. We also observed several small (< 200 μm) fragments of silicic-K-feldspar intergrowths within the meteorite matrix, rare small (< 200 μm) glass beads and amorphous glass clasts confirming that the sample was derived from an immature lunar regolith source (Wentworth and McKay 1990; Eugster et al. 1991; Taylor 1991).

Both MAC 88105,159 and MAC 88104,47 are dominated by abundant impact clasts that range in size from very large (approximately 5 mm in diameter) fragments to small fragments indistinguishable from the matrix construct. The majority of these clasts are impact melt breccias with clastic textures (Fig. 3l) formed of plagioclase and rarer olivine grains bound by a mafic aphanitic/amorphous mafic glass matrix. Microcrystalline impact melts, where present, have a plumose texture indicative of rapid quenching.

The majority (11 of 16 analysed in this study) of melt clasts are feldspathic normative noritic anorthosite (> 26 wt% Al_2O_3, < 15.5 ppm Sc; Fig. 5), similar to those feldspathic melt clasts in MAC 88105 described by Jolliff et al. (1991). Taylor (1991) classifies these aluminous melt breccias as being akin to the group 3 Apollo 16 melt samples (McKinley et al. 1984; Korotev 1994), however the results of our trace element studies indicate that feldspathic impact melt and breccia clasts in MAC 88104/05 (Tables 2 and S1) are generally ITE-poorer than group 3 melts (approximately 2.5 to 3.5 Sm ppm) and are more akin to the group 4 feldspathic varieties (Fig. 6e, Table 2).

We identify three sub-groups of feldspathic melts where MAC type 1 clasts have the lowest REE concentrations ($\times 2_{cn}$–$\times 4_{cn}$ for the trivalent REE); MAC type 2 feldspathic melts comprise a group of nine clasts with similar REE patterns ($\times 6_{cn}$ to $\times 11_{cn}$ for the trivalent REE), major element and Mg# values (Table S1: $Mg\#_{57\text{-}60}$, mean $Mg\#_{59}$); and MAC type 3 is represented by one clast in the MAC 88105,129 with similar low-ITEs to the MAC type 1 impact melts but with comparatively a lower CaO abundance (16.2 wt%), higher Mg/Fe ratios ($Mg\#_{66}$) and Cr concentrations (1188 ppm) (MAC type 1 impact melts have 17.8 wt% CaO, $Mg\#_{56}$ and 455 ppm Cr).

In our MAC 88104/05 sections we found no examples of basaltic melt with high K/P ratios, which are interpreted by Taylor (1991) to be indicative of melt sheet late-stage liquid immiscibility. However, one feldspathic (noritic anorthosite normative) clast in MAC 88105,129 (High-ITE clast: Tables 2 and S1) has anomalously high ITE concentrations (3.3 ppm Th, 17.5 ppm Sm, $\times 53_{cn}$ to $\times 146_{cn}$ trivalent REE: Figs. 6e and 7d) and a negative Eu-anomaly (Eu/Eu* 0.33).

Three impact melt clasts in MAC 88104,47 are mafic (< 19 wt% Al_2O_3, < 15.5 ppm Sc, equivalent to normative anorthositic norite; Fig. 5), with lower Mg# values ($Mg\#_{50\text{-}56}$) and more Sc, Ti, Cr, Mn, and REE compared with MAC 88104/05 feldspathic melts (Table S1, Figs. 6a and 7d). These have micro-crystalline plagioclase laths and a pyroxenous glass matrix, sometimes containing partially melted relict clasts of pyroxene, ilmenite, and plagioclase (as shown in Fig. 3k). Like basaltic melts seen in other sections of MAC 88105 (Jolliff et al. 1991; Taylor 1991) and the anorthositic Yamato-791197 lunar meteorite (Lindstrom et al. 1986) these impact melts and breccias are more ferroan, and Sc-richer than Apollo mafic impact melts (Jolliff 1998; Korotev 2000).

Impact Glass Composition

Glass impact spheroids (beads) and amorphous fragments are distributed heterogeneously throughout the matrix of PCA 02007, MAC 88104/05, and MET 01210. Spherical beads and fragmented beads (those broken by comminution processes) range in size from < 20 μm to 1 mm and have a range of textures from homogenous glass to those with devitrified micro-crystalline inclusions (Fig. 3i). We discriminate impact glass from pristine volcanic picritic glass following the guidelines of Levine et al. (2005). Volcanic glass consistently have > 1.1 Mg/Al ratios (based on compositions of groups listed in the electronic appendix A3.12 of Wieczorek et al. 2006 and Clive Neal's "Mare Basalt Database" available as an electronic appendix to Jolliff et al. 2006), so we classify any impact glass in our meteorites with < 1.1 Mg/Al element ratios as having an impact origin.

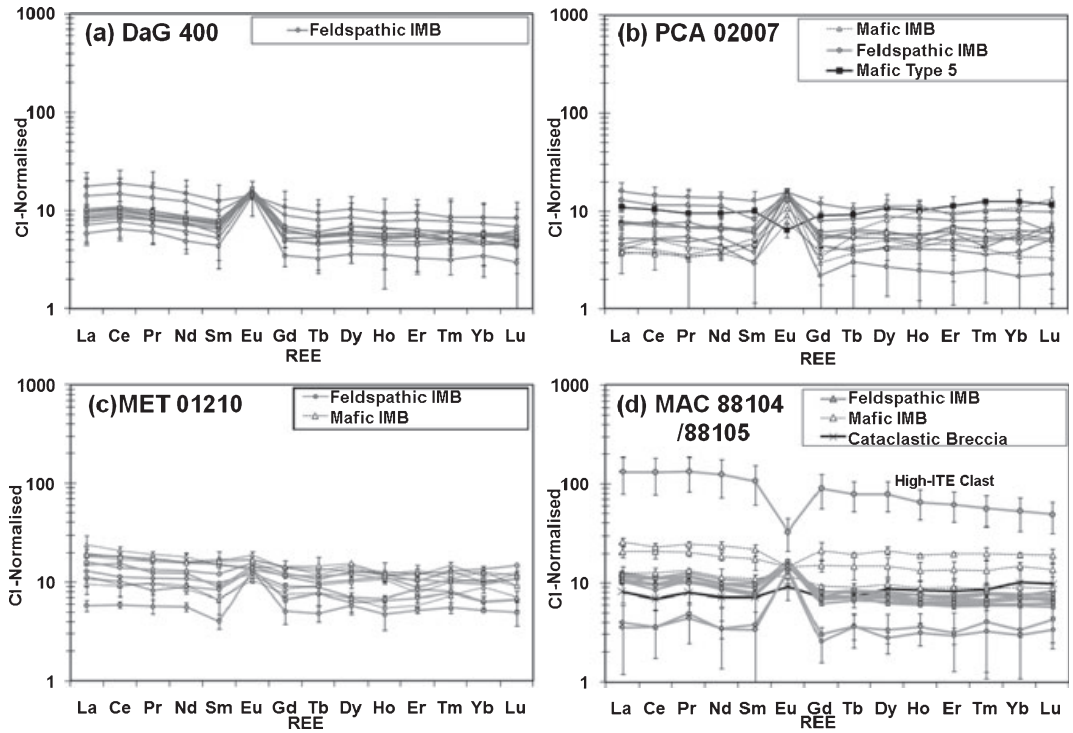

Fig. 7. Chondrite-normalized (Anders and Grevesse [1989]) REE patterns in individual impact melt and melt breccia clasts (summarized as IMB) in a) DaG 400 b) PCA 02007, c) MET 01210, and d) MAC 88104/05. Element concentrations are listed in Table S1. Error bars shown are 2σ.

The majority of beads and impact melt glass analysed in MET 01210, PCA 02007, and MAC 88104/5 (see also Delano 1991; Taylor 1991; Warren et al. 2005; Day et al. 2006; Korotev et al. 2006) are aluminous in nature and most similar in composition to low-Ti beads from the Apollo 16 landing site (Naney et al. 1976; Kempa and Papike 1980). Beads with slightly more TiO_2-rich compositions (>2 wt% TiO_2) are likely derived from impacts in protoliths with Ti-bearing mineral phases (ilmenite, ulvöspinel), suggesting melting and mixing of low-Ti mare basaltic lithologies and more aluminous feldspathic protoliths (Fig. 8).

Rare glass and bead fragments have compositions with less SiO_2 relative to beads collected at the Apollo landing sites (Fig. 8). In particular one large anhedral glassy aggregate and one small bead in MET 01210,21 and one fragment in MAC 88105,159 have low-FeO (0.17–6.7 wt%), high-CaO (21–25 wt%) and Al_2O_3 (32–42 wt%) concentrations similar to HASP (High-Aluminum, Silica-Poor) glass identified at the Apollo 14 and 16 landing sites (Naney et al. 1976; Vaniman and Bish 1990; Papike et al. 1997). These HASP beads are thought to represent impact-induced volatilisation products, where SiO_2 and FeO are preferentially lost relative to Al_2O_3 content from a feldspathic (probably near-pure anorthosite) protolith (Naney et al. 1976; Papike et al. 1997).

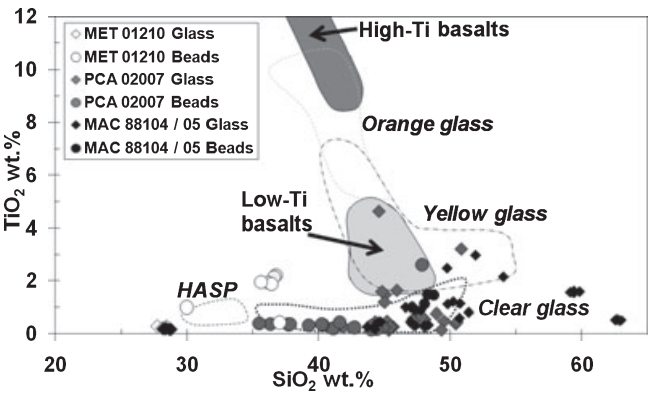

Fig. 8. Comparison of glass bead compositions found in matrix of MET 01210, PCA 02007, and MAC 88104/05 compared with Apollo 16 soil and regolith glass fragments (adapted from Fig. 3 of Naney et al. [1976]). HASP = high alumina, silica poor glass.

DISCUSSION

Constraining the Source Region of DaG 400, MET 01210, PCA 02007, and MAC 88104/05

Constraining the source provenance of lunar meteorites helps to provide a direct link between laboratory analysed lunar samples and the wider geological context of their source regions. The regolith

breccias discussed here likely originate from within a few tens of meters of the surface of the Moon (Warren 1994). Therefore, regolith compositions estimated from optical spectroscopy techniques (e.g., Lucey et al. 2000), which only sample to a depth of approximately 1 micron into the lunar surface (Lucey et al. 2006), are not ideal for this type of investigation. Instead, we have used gamma-ray spectroscopy data, which measures the upper few centimeters to meters of regolith chemistry (Prettyman et al. 2006 and references therein), to search for regions that are compositionally similar (Fig. 11) to the bulk FeO and Th composition of the meteorites in this study (Table 3 and see Fig. 11 caption for methodology). For this study we have utilized the Lawrence et al. (2003) 0.5° (15 km) per pixel Th ppm, and Lawrence et al. (2002) 0.5° per pixel FeO data sets.

DaG 400

Remote sensing observations interpretations have shown that the lunar farside highlands are dominated by Th-poor (KREEP-poor), feldspathic rocks (Jolliff et al. 2000; Prettyman et al. 2006). Many previous studies (e.g., Palme et al. 1991; Korotev et al. 2003; Korotev 2005) have concluded that feldspathic lunar meteorites likely originate from the farside Feldspathic Highlands Terrane (FHT) and the Outer-Feldspathic Highlands Terrane (FHT-O: as defined by Jolliff et al. 2000) and results of our study (Fig. 11) are consistent with these conclusions: we show that DaG 400 was most likely launched from a regolith within the central farside FHT or the western and eastern regions of the FHT-O.

MET 01210

This meteorite was sourced from a regolith originating in a mixed highlands-mare region of the Moon (Day et al. 2006; Fig. 12 of Joy et al. 2008; Korotev et al. 2009; Arai et al. 2010). The bulk sample (Table 1) and impact melt clasts (Table S1) are ITE-poor (Table 1) indicating that it was not likely sourced from the Th-rich Procellarum KREEP Terrane. Arai et al. (2010) propose that MET 01210 could have originated from a small 1.4 km crater within the Schickard crater floor on the nearside of the Moon, however on the scale (0.5°/pixel) of the Lunar Prospector data used in our study, the region in the vicinity of their proposed crater at 53°W, 44.5°S has too low an FeO content (8.2–8.6 wt% FeO: Lawrence et al. 2002) to be similar to the bulk sample (16.5 wt% FeO: Tables 1 and 3). Our results (Fig. 11b) instead suggest that the meteorite could have been launched from a regolith located in (1) Mare Crisium; or (2) discrete regions of north-eastern and south-eastern Mare Tranquillitatis; or (3) north-westerly regions of Mare Fecunditatis (Fig. 11). However, we deem it unlikely that MET 01210 is from the north-eastern part of Mare Tranquillitatis, as this area is dominated by high-Ti mare basalts (i.e., see Clementine TiO_2 map of Lucey et al. 2000) and not the low-Ti and VLT mare basalts (Day et al. 2006) and low-Ti impact melts (Fig. 6a) sampled by the MET 01210 regolith. The potential source regions we have identified in Mare Crisium and Mare Fecunditatis (Fig. 11b) have low TiO_2 concentrations that are more akin to the MET 01210 regolith (1.55 wt% TiO_2: Table 1). Moreover, these areas are also located in close proximity to feldspathic highlands regions, consistent with the feldspathic clasts included in the sample (Figs. 1c and 1d, see also Day et al. 2006). However, we note that crater counting ages for these regions indicate that lava flows could be marginally too young (approximately 3.5–3.75 Ga for Mare Crisium; Boyce and Johnson [1977]; and approximately 3.5–3.7 Ga for the northern [F1] units of Hiesinger et al. [2006]) to have been the source of the MET 01210 basalt fragments that crystallized at approximately 3.85 Ga (Terada et al. 2007a).

PCA 02007 and MAC 88104/05

These meteorite have low bulk rock ITE concentrations (Table 1), suggesting that they were formed in regoliths distal to the nearside PKT. Possible PCA 02007 source regoliths include regions within the farside FHT, farside FHT-O, and some FHT-O localities in the nearside southern highlands (Fig. 11c). MAC 88104/05 is reported to have been launched from the Moon 0.26–0.29 million years ago (Nishiizumi et al. 1991). The meteorite has a marginally higher bulk Th concentration than PCA 02007 (Table 1), and as such it unlikely that the meteorite sampled Th-poor (< 0.4 ppm Th) regions of the central FHT. Our results constrain MAC 88104/05 to be most compositionally similar to FHT-O environments including the south polar highlands area, highlands south of Tycho crater, farside far northern highlands and feldspathic terranes surrounding Mare Australe (Fig. 11d).

Meteorite Bulk Sample and Impact Melt Composition: Comparison with Lunar Samples

Our DaG 400, MET 01210, PCA 02007, and MAC 88104/88105 bulk compositions are listed in Table 1, and illustrated in Figs. 5, 6, and 9, where they are compared with Apollo rock suites and other reported lunar meteorite bulk compositions.

DaG 400

Our DaG 400 bulk composition (Table 1, Fig. 9) is similar to those reported from other chips of DaG 400 using different geochemical techniques (Zipfel et al. 1998; Korotev 2005; Warren et al. 2005). However, in

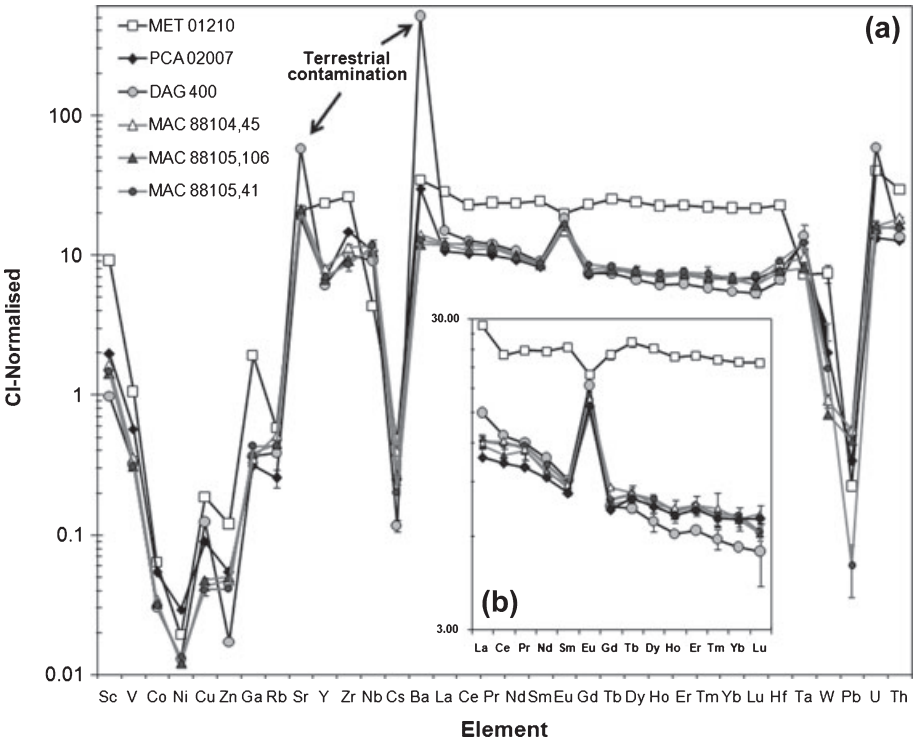

Fig. 9. a) CI-normalized (Anders and Grevesse [1989]) bulk sample composition of the meteorites examined in this study (Table 1). Note that Sr and Ba values reported in DaG 400 represent terrestrial contamination rather than lunar values. b) Inlay shows detail of bulk REE concentrations. Error bars are 2σ and are typically smaller than the spot size.

comparison to these studies our bulk P_2O_5 wt% composition (0.42 wt% P_2O_5) is ×2 to ×4 higher than literature values (0.11–0.22 wt% P_2O_5), suggesting that our value may be anomalous. Our bulk rock analyses also shows an enhancement of Ba (1203 ppm) and Sr (451 ppm) compared with literature data (140 to 820 ppm Ba, 190 to 300 ppm Sr) indicating that our bulk sample chip was likely taken from a region of the meteorite with enhanced terrestrial mineralisation. Our data also has slightly elevated ITE concentrations, representing about a 1% KREEP addition (using the high-K KREEP values of Warren 1989), indicating that we may have sampled a subsection of DaG 400 that was dominated by the ITE-richer feldspathic impact melt we identify in this study (DaG type 3: Table S1).

The majority of impact melt and melt breccia clasts in DaG 400 (see also Cohen et al. 1999) have a limited range of major (Table S1, Figs. 5 and 6) and trace element (Fig. 7a) composition. We identify ten clasts in our section of DaG 400 that form a main group of feldspathic impact melt (DaG type 2). The mean composition of this group of impact melt (Table 2) is comparatively more ferroan and has higher concentrations of Sc and Th/Sm than the DaG 400 bulk rock (DaG type 2 clasts = $Mg\#_{66}$, 8.7 ppm Sc, 1.8 Th_{cn}/Sm_{cn}; DaG 400 bulk rock = $Mg\#_{71}$, 5.7 ppm Sc, 1.5 Th_{cn}/Sm_{cn}). These differences are consistent with the bulk rock containing a nonimpact ferroan anorthosite and/or magnesian anorthosite component with higher Mg# values and lower Sc concentrations.

The DaG type 2 feldspathic impact melt group has a similar range of Sm and Sc concentrations (Table S1) to "ungrouped" feldspathic impact melt from sample 65758 (where 65758 fragments have < 2 ppm Sm and 7.5–8.5 ppm Sc: Korotev 1994). They are also similar in composition to that of the average composition of lunar feldspathic meteorites (table 5 of Korotev et al. 2003). We therefore interpret that these clasts originate from a single impact into the upper few kilometers of typical feldspathic lunar crust (as listed in table 5 of Korotev et al. 2003). The DaG 400 parent regolith was then likely formed on top on this impact melt sheet and primarily sampled this material.

The other two groups of DaG 400 impact melt were likely ejecta derived from other impact events into local feldspathic targets. The DaG 400 type 3 impact melt can be explained by mixing typical feldspathic upper lunar crust with a 1 to 2% additional high-K KREEP component (Warren 1989). The Dag type 1 impact melt breccia is consistent with mixing between feldspathic upper lunar crust and approximately a 40% additional ferroan anorthosite component (where the FAN

component had a mid range Mg# with high Sc/Sm ratio and low Th_{cn}/Sm_{cn} ratio).

MET 01210

Meteorite Hills 01210 has an intermediate FeO and Al_2O_3 bulk rock composition resulting from the mixture of low-Ti mare basalt, very low-Ti (VLT) mare basalt and ferroan anorthosite lithic and granulitic material (Day et al. 2006; Joy et al. 2008; Arai et al. 2010). It has been proposed that MET 01210 represents a regolith overlying the basaltic flows that was the source of the low-Ti/VLT basaltic lunar meteorites Yamato-793169, Asuka-881757 and MIL 05035 (Yanai et al. 1993; Day et al. 2006; Nishiizumi et al. 2006; Arai et al. 2007, 2010; Joy et al. 2008; Fernandes et al. 2009; Liu et al. 2009): this group of meteorites is referred to as the Y/A/M/M group. Whilst lying on top of these lavas, the regolith must have also been proximally located to FAN bedrock to amass its feldspathic clast contribution (Fig. 12; see also Joy et al. [2008] and Arai et al. [2010]).

We have identified both feldspathic and mafic impact melt and melt breccia clasts in MET 01210 (Tables 2 and S1). A simple mixing calculation suggests that the mafic impact melt mean composition (Table 2) is consistent with mixing between (1) approximately 70% typical upper feldspathic crust (Korotev et al. 2003) with (2) approximately 2% KREEP addition (high-K KREEP of Warren 1989), and (3) approximately 28% low-Ti basalt akin to the average composition of Yamato-793169/Asuka-881757/MIL 05035. The mean composition of the feldspathic impact melts and melt breccias (Table 2) is similar to the compositions of feldspathic impact melts from the DaG type 2, PCA type 2, and MAC type 2 groups (Table 2), although in comparison to these groups, the MET type 1 feldspathic group has higher concentrations of TiO_2, Sc, REE, and Th (Fig. 10, Table 2), which is akin to the minor and trace element chemistry of Luna 20 feldspathic impact melt breccia 22023,18B (Swindle et al. 1991).

PCA 02007

Pecora Escarpment 02007 contains an anorthositic clast component, which is more magnesian than Apollo FAN samples (Korotev et al. 2006), and is dominated by impact melt and melt breccia clasts (Fig. 1b, see also Day et al. [2006] and Korotev et al. [2006]). For major elements, our bulk rock composition (Table 1) agrees well with the values reported by Korotev et al. (2006) but differs, particularly for SiO_2, FeO and Al_2O_3 values to that of Day et al. (2006). For minor and trace elements (Table 1), our values are similar to those reported in these previous studies, although, our bulk

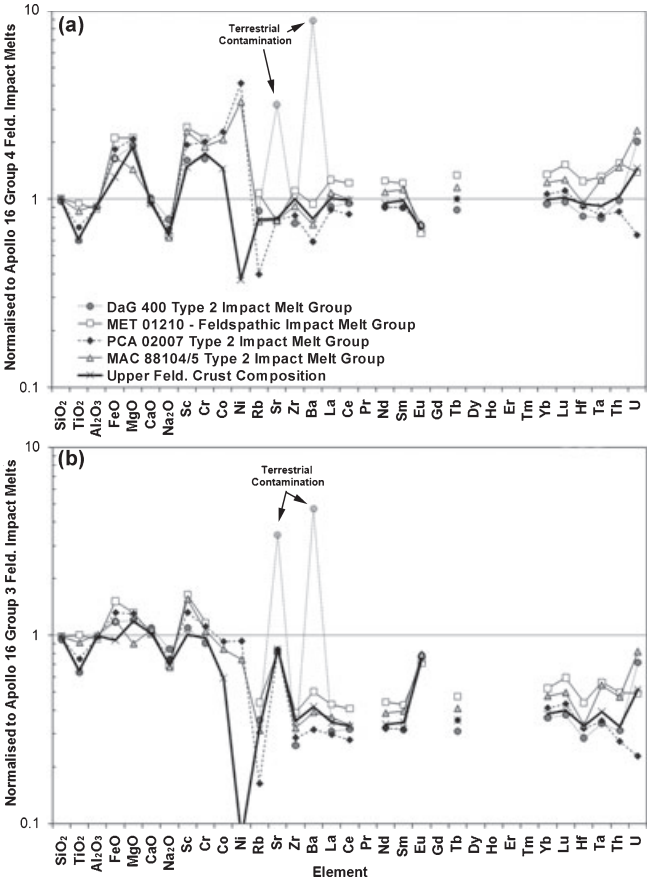

Fig. 10. Average lunar meteorite feldspathic impact melt group compositions (Table 2) normalized to a) the mean composition of the Apollo 16 group 4 feldspathic impact melt (Korotev 1994) and b) the mean composition of the Apollo 16 group 4 feldspathic impact melt (Korotev 1994). Note that Sr and Ba values reported in DaG 400 represent terrestrial contamination rather than lunar values. The estimated composition of the upper few kilometers of the lunar crust is taken from table 5 of Korotev et al. (2003).

Cr (941–1168 ppm) is notably higher than most feldspathic lunar meteorites (typically $< < 1000$ ppm Cr) and to that reported by Day et al. (2006) for PCA 02007 (660 ppm Cr). Korotev et al. (2006) also report that PCA 02007 has a high Cr content (1074 ppm Cr) that is within the range of our measurements. They estimate that 9% of the Cr in PCA 02007 could have been contributed from exogenous meteoritic material. However, if we correct for this 9% meteorite added Cr, our and Korotev et al.'s (2006) PCA 02007 Cr concentrations (856–1063 ppm) are still much higher than the estimated composition of the upper feldspathic lunar crust (630 ppm Cr: Korotev et al. 2003) indicating that our sampled portions of the meteorite could contain an additional Cr-rich endogenic component to account for this discrepancy.

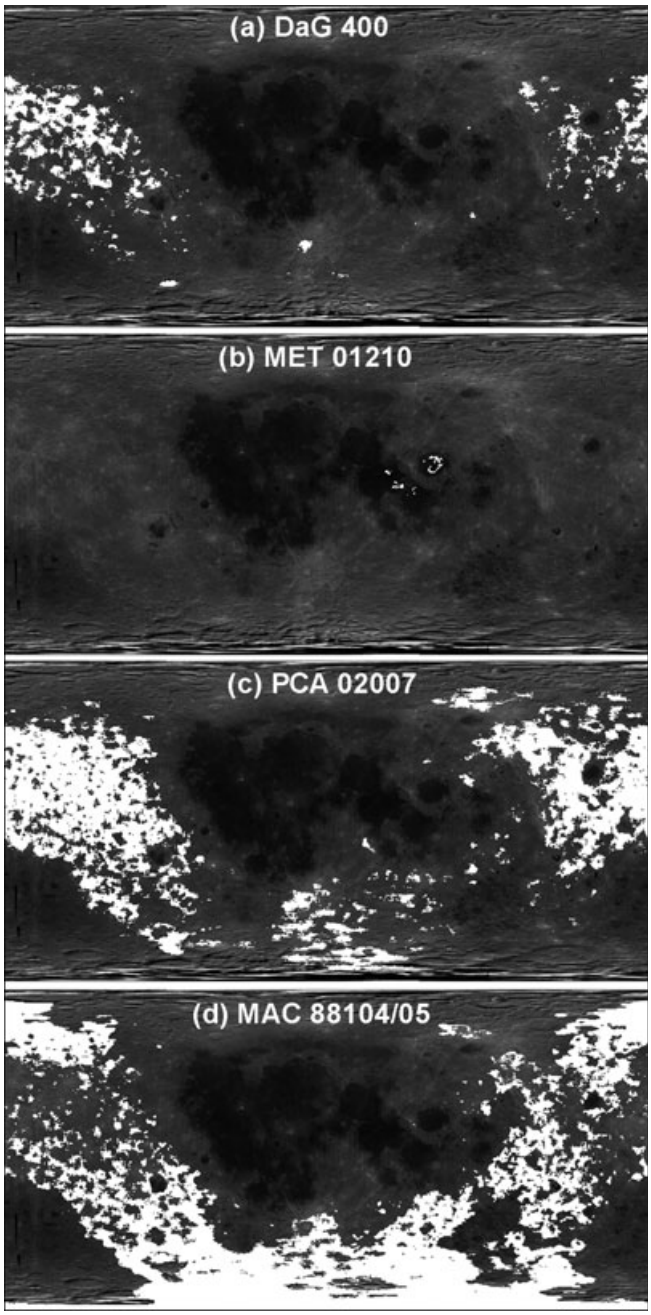

Fig. 11. Identification of lunar regoliths with most similar compositions to the meteorites in this study. The bulk meteorite Th ppm and FeO wt% concentrations (Table 1) were used to define two input "composition parameters" for each meteorite (Table 2). To account for small errors in the bulk composition analyses (Table 1), and the remote sensing data set used in this study, two "compositional range" parameters were then defined as "meteorite Th ppm concentration ± 1 ppm" and "meteorite FeO wt% concentration ± 1 wt%." Table 2 lists these "compositional range" parameters for all four meteorites. The Lunar Prospector 0.5° per pixel 360° × 180° Th ppm (Lawrence et al. 2003) and FeO wt% (Lawrence et al. 2002) data sets (each data set contains 259200 individual pixel information) were then searched for pixels with compositions within the defined "compositional range" (using an interface description language [IDL] programme written by K. Joy). Pixels that fulfilled both the Th and FeO "compositional range" criteria were denoted as "region of interests" and we interpret these localities as the most compositional similar terrane to the input meteorite composition (± error factor). Pixels that denote "region of interests" are colored white for each meteorite a) DaG 400, b) MET 01210, c) PCA 02007, and d) MAC 88104/05 and are overlain on a geographically corresponding Clementine cylindrical projection albedo map of the Moon (USGS, Map a Planet).

In PCA 02007 there appears to be at least two compositional groups of feldspathic impact melt and melt breccia (PCA type 1 and PCA type 2: Fig. 6, Table S1). We interpret that PCA type 1 was likely was formed by an impact into ferroan anorthositic crust containing very low quantities of mafic, KREEP or meteoritic components. PCA type 2 feldspathic impact melt, represented by ten noritic anorthosite normative clasts, has similar Mg#, Sc and ITE concentrations but lower concentrations of transition elements (Cr-Zn) than the PCA 02007 bulk rock composition (Tables 1 and 2). This difference is consistent with the feldspathic impact melt not containing such a high level of meteoritic material (Korotev et al. 2006 estimate a 2.7–2.8% chondritic meteorite component in PCA 02007) or Cr-rich mafic material (see below) as the PCA 02007 bulk rock.

The mafic melts are subdivided into three groups based on their Mg# content and their Sc, Cr, Ni, REE

Table 3. Compositional range Th and FeO conc.s for DaG 400, MET 01210, PCA 02007, and MAC 88104/05 based on the measured bulk-rock compositions listed in Table 1. Note that the MAC 88104/05 starting compositions for Th and FeO are derived from average of the three bulk measurements listed in Table 1 (for MAC 88104,45, MAC 88105,106, and MAC 88105,41). comp = Compositional. and conc = concentration.

	DaG 400			PCA 02007			MET 01210			MAC 88104/5		
Element	Comp. range min.	Measured conc.	Comp. range max.	Comp. range min.	Measured conc.	Comp. range max.	Comp. range min.	Measured conc.	Comp. range max.	Comp. range min.	Average conc.	Comp. range max.
Th (ppm)	0.00	0.39	1.39	0.00	0.37	1.37	0.00	0.86	1.86	0.00	0.49	1.49
FeO (wt%)	2.61	3.61	4.61	5.30	6.30	7.30	15.46	16.46	17.46	3.43	4.43	5.43

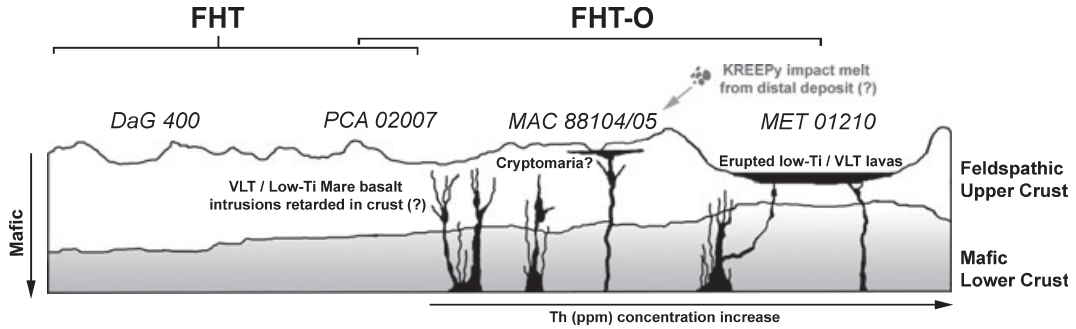

Fig. 12. Cartoon to illustrate the possible lunar launch localities of the meteorites analysed in this study. Lunar lithologies contributing to each meteorite are inferred from regolith lithic clast type and from composition of impact melt breccias. Diagram is schematic. FHT = Feldspathic Highlands Terrane (Jolliff et al. 2000). FHT-O = Outer Feldspathic Highlands Terrane (Jolliff et al. 2000).

concentrations (Tables 2 and S1). PCA type 3 impact melt is characterized as a normative anorthositic norite with $Mg\#_{62}$. PCA type 4 mafic impact melt is similar in composition to the PCA type 3 group, although is comparatively more pyroxenous (norite normative with a lower La/Yb ratio), more ferroan ($Mg\#_{52}$) and has higher concentrations of Sc, Ti, Mn, and Cr. It is plausible that the two groups originate from the same impact melt sheet and represent different degrees of mixing between (1) a KREEP-poor, feldspathic target and (2) a KREEP-poor, ferroan, pyroxenous, target that has high Cr concentrations, Sc/Sm, low Th_{cn}/Sm_{cn} and La/Yb ratios akin, but not identical, to the Kalahari 009 basaltic lunar meteorite (Sokol et al. 2008).

The PCA type 5 mafic group (Table 2) is norite normative and with $\times 6_{cn}$–$\times 12_{cn}$ trivalent REEs, a negative Eu anomaly ($Eu/Eu^* = 0.7$) and has higher Th_{cn}/Sm_{cn} ratios, lower Eu/Sm, higher Cr-concentration than the other PCA mafic melts (Fig. 6), suggesting a different crater origin. Ni contents in the clast are relatively low (40 ppm) compared with Apollo mafic melts (>160 ppm Ni: Jolliff 1998) indicating negligible meteoritic addition; for example a 1% addition of CI or CM or CO chondrites would potentially add 107–140 ppm Ni to the impact melt (based on the average chondrite meteorite Ni values listed in Wasson and Kallemeyn 1988). Therefore, we propose that this type of mafic impact melt might be the contributing factor to high Cr concentrations in the bulk rock sample, rather than solely a meteoritic addition as suggested by Korotev et al. (2006). A simple mixing model suggests that the composition of this mafic sample is consistent with impact melting of approximately 97% VLT basaltic bedrock with a mid range Mg# value, a high Cr content and high Sc/Sm ratio (Fig. 6) mixed with approximately 1% high-K KREEP (Warren 1989) and a minor (approximately 2%) feldspathic component. We propose that it is possible that the target basaltic rock type was akin to Cr-rich (>4000 ppm) olivine VLT vitrophyre basalt (i.e., like samples 70006 and 70007: Wentworth et al. 1979).

MAC 88104/05

Our bulk measurements of MAC 88104/05 are generally consistent for each element analysed (Table 1). We note that the K_2O wt% content of MAC 88104,45 (Table 1) is about ×4 higher than values reported for MAC 88104/05 by other workers (Neal et al. 1991; Jolliff et al. 1991; Koeberl et al. 1991; Lindstrom et al. 1991; Palme et al. 1991). This discrepancy is also seen in elevated P_2O_3, Zr, and Th concentrations in MAC 88104,45 (Table 1), suggesting that this chip may have sampled a marginally KREEP-richer component than other sub-splits. Compared with bulk composition of the DaG 400 and PCA 02007 feldspathic lunar meteorites (Table 1), the MAC 88104/05 meteorite is more ferroan and aluminous, indicating that it contains a higher modal ferroan anorthosite clast and mineral component.

The three groups of feldspathic melt in MAC 88104/05 (MAC type 1, type 2, and type 3: Table 2) are compositionally distinct (Fig. 6) and we suggest they were derived from at least three impact melt sheets. We note that the MAC type 3 group is similar in composition to the bulk compositions of the Kalahari 008 (Sokol et al. 2008), NWA 3163/4483 (Korotev et al. 2008) and Yamato-86032/82192/82193 feldspathic lunar meteorites (Koeberl et al. 1989).

The MAC type 2 feldspathic impact melt group consists of nine clasts. Compared with the MAC 88104/05 bulk rock composition (Table 1), this group (Table 2) is more ferroan with higher concentrations of Ti, Sc and higher La/Yb ratios, indicating an additional pyroxene component. The group is within the spread of

feldspathic lunar meteorite bulk compositions and the MAC type 2 group is more ferroan ($Mg\#_{59}$), is Sc-richer (12.3 ppm Sc), and has slightly higher REE concentrations ($\times 7_{cn}$–$\times 11_{cn}$ for the trivalent REE) than feldspathic groups in DaG 400 and PCA 02007 (Table 2). These differences are consistent with the MAC type 2 melts being formed by melting comparatively ferroan anorthositic target with a minor additional ferroan-mafic component.

The lone ITE-rich feldspathic fragment in MAC 88105,159 (MAC type 4) is more aluminous than KREEPy impact melts collected at the Apollo 16 landing site (i.e., the group 1 compositional group: Fig. 5). The clast trace element data is consistent with a mixture of approximately 67% feldspathic upper crust (Korotev 1994), approximately 29% high-KREEP component (Warren 1989) with a minor 1% meteoritic (i.e., CI chondrite: Anders and Grevesse [1989]) and approximately 4% low-Ti basalt contribution. The fragment likely originated from distal KREEP-rich target and was introduced into the MAC 88104/05 parent regolith as "exotic" impact ejecta fragment.

The mafic impact melt clasts (MAC type: Table 2) analysed in MAC 88104,47 have similar clast-poor crystalline textures, similar quantities of V, Mn, Cr, and low ITE-concentrations (variation in REE trends is caused by minor variations in modal pyroxenous mafic glass and plagioclase content). A simple mixing model indicates that this mafic melt group is consistent with being derived from an impact into a mixture of (1) approximately 28% typically upper feldspathic crust and (2) approximately 69% KREEP-poor low-Ti basaltic target and (3) approximately 2% high-ITE lithology (high-K KREEP: Warren 1989) and (4) approximately 1% CI meteoritic material (Anders and Grevesse 1989).

Meteorite Impact Melt Composition: Implications for the Composition of the Lunar Crust

Impact melt clasts in these four meteorites are distinct from Apollo melt rock by their lower abundances of incompatible trace elements, like those in KREEP (Korotev 1994; Jolliff 1998). Thus, it seems certain that these meteorites formed distally from the Procellarum KREEP Terrane (Fig. 11), which is characterized by high surficial Th-contents (Jolliff et al. 2000; Lawrence et al. 2002, 2003), or prior to the expression of this Terrane. Further, impact melt and melt breccias in these meteorites are too ferroan, rich in Sc and ITE-poor to contain significant proportions of nearside lithologies like Magnesian Suite plutonics or the High-Alkali Suite (Jolliff 1998; Korotev 2000). In this section, we discuss mixing relations among likely chemical components in the melt rock clasts, and the geological settings that they likely represent.

Mixing Between Feldspathic Crust and Ferroan Low-Ti/VLT Basaltic Crust: The Nature of the Outer Feldspathic Highlands Terrane

Three of the four meteorites studied here were sourced from regions with both feldspathic highlands and basaltic rock types (Figs. 11 and 12). The mafic impact melt groups described here (MET type 2, PCA type 3, 4, and 5 and MAC type 5: Table 2) are also consistent with impact mixing between feldspathic material (either typical upper crust material, Korotev et al. 2003; or more pristine ferroan anorthosite targets) with a mafic component similar to KREEP-poor low-Ti and VLT basalts from the Apollo, Luna, and lunar meteorite collection (Fig. 6).

For the mafic melts in MET 01210 (Table 2), the basaltic end-member is indistinguishable from the average composition of the grouped stones Yamato-793169, Asuka-881757, and MIL 05035. So we interpret that these impact melts were formed by small local impacts melting and mixing into the Y/A/M/M lava flows (approximately 28%) with underlying feldspathic upper crust material (approximately 70%) and a minor component of ITE-rich material (approximately 2% high-K KREEP: Warren 1989).

The feldspathic meteorites PCA 02007 and MAC 88104 contain mafic impact melts consistent with mixing between feldspathic lithologies and different types of VLT to low-Ti basalts. Clasts of such basalts (and mineral fragments from them) are present in many lunar meteorites (Fig. 1 of this study, Goodrich and Keil 1987; Lindstrom et al. 1986; Taylor 1991; Jolliff et al. 1991; Koeberl et al. 1991; Korotev et al. 1996; Day et al. 2006; Robinson and Treiman 2010).

PCA 02007 and MAC 88105 are inferred (Figs. 11 and 12) to have been sourced from the Outer Feldspathic Highlands Terrane. However, this terrane shows few exposures of mare basalts. Thus, the presence of mafic impact melts in these meteorites, and rare basalt fragments, is consistent with Basilevsky et al. (2010) and with other inferences that the FHT-O likely contains a fraction of buried VLT/low-Ti basalts (i.e., cryptomaria: Hawke et al. 1985; Antonenko et al. 1995; Campbell and Hawke 2005; Hawke et al. 2005; Terada et al. 2007b; Arai et al. 2010) and/or shallow basalt intrusions (Head and Wilson 1992).

The Nature of the Lunar Feldspathic Crust

Remote sensing studies show that the lunar primary crust is compositionally heterogeneous and is most likely a composite of upper anorthositic and lower more mafic (i.e., noritic, gabbroic and/or troctolitic) crustal

lithologies (e.g., Spudis and Davis 1986; Jolliff and Haskin 1995; Pieters and Tompkins 1999; Bussey and Spudis 2000; Wieczorek and Zuber 2001; Korotev et al. 2006; Shearer et al. 2006; Arai et al. 2008), which were subsequently intruded by magmatic suites (Head and Wilson 1992; Shearer and Floss 2000).

Basin forming and other large impacts into the feldspathic highland crust will most likely produce feldspathic KREEP-free impact melt (Korotev et al. 2006), representative of the nature of the crust up to tens of kilometers below the target area (Stöffler et al. 2006). Feldspathic impact melts were extensively sampled by the Apollo 16 mission in the central nearside highlands, where impact melt rocks represent mixing between low-Th and high-Th rocks (Korotev 2000). The most KREEP-poor impact melt returned by Apollo 16 are the ferroan group 4 feldspathic impact melts (Table 2) including anorthosite normative, fragment laden, microporphyritic, and intergranular-textured melt breccias (Floran et al. 1976; Lindstrom and Salpas 1982; McKinley et al. 1984; Spudis 1984; Korotev 1994). Korotev (1994) reports that the majority (approximately 97%) of the rock fragments comprising this group represent ejecta from the local North Ray crater (approximately 1 km in diameter; Lindstrom and Salpas 1982), which 50 Ma ago (Arvidson et al. 1975) is assumed to have excavated a >4.1 Ga anorthositic target rock (Reimold et al. 1985). The other main group of feldspathic impact melt collected at Apollo 16 are the group 3 impact melts, comprised of clast-poor, intersertal melt rocks (Korotev 1994). These are noritic anorthosite normative, are less aluminous than the group 4 melts (Fig. 5), and have higher ITE and Sc-concentrations (Table 2). These impact melts are inferred by Korotev (1994) as having formed from one or several small (5 to 7 km: Deutsch and Stöffler 1987) impacts into feldspathic upper crust between 3.75 Ga (Deutsch and Stöffler 1987) to 3.84 Ga ago (McKinley et al. 1984).

The main groups of feldspathic impact melt and melt breccias in our study have major element compositions and Sc, Cr, Co, and Ni concentrations similar to the Apollo 16 group 3 melt group (Fig. 10b, Table 2). However, conversely our impact melts have Rb, Zr, Ba, and ITE concentrations more akin to Apollo 16 group 4 melt group (Figs. 6e and 10a), indicating that the feldspathic clasts analysed in this study represent melting of KREEP-free rocks. This trend is also seen in (1) feldspathic impact melt clasts and anorthositic fragments from other lunar meteorites (e.g., Goodrich et al. 1984; Lindstrom et al. 1986; Taylor 1991; Cahill et al. 2004; Korotev et al. 2006; Nyquist et al. 2006); (2) lunar meteorite impact melt breccias NWA 482 and Dhofar 026 (Warren et al. 2005); and (3) estimates of the composition of the lunar feldspathic crust (table 5 of Korotev et al. 2003; and see Fig. 10 of this study). Moreover, compared with the Apollo 16 group 3 and 4 groups (Fig. 10; Table 2), the feldspathic impact melt groups from our study have notably lower (i.e., by 60% to 80%) concentrations of Sr (with the exception of the DaG 400 clasts, which are terrestrially contaminated) and Eu (Fig. 10; Table 2). This is also seen in feldspathic impact melt in other lunar meteorites (e.g., MAC 88105: Neal et al. 1991; Yamato-82192: Warren and Kallemeyn 1987; ALH 81005: Goodrich et al. 1984; NWA 482 and Dhofar 026: Warren et al. 2005).

These results are consistent with the bedrock sources of the meteorite impact melts being less anorthositic than the PreNectarian crust melted to form the Apollo 16 group 4 impact melts. This might be taken to imply that the central nearside crust sampled at the Apollo 16 site is richer in ferroan anorthosite compared to the sources of the feldspathic lunar meteorites (Korotev 1996, 1997), and indeed recent remote sensing data (Ohtake et al. 2009) have identified near-surface outcrops off essentially pure anorthosite (PAN) at the nearby South Ray crater. However this does necessarily imply that the central near-side crust as a whole is more anorthositic than elsewhere. For example, the impacts responsible for producing the meteorite impact melt groups may have penetrated to a deeper, more mafic (e.g., noritic) crustal layer than the relatively small impacts which appear to be responsible for the Apollo 16 group 3 and 4 materials (Korotev 1994). Conversely, a similar result might be obtained if the meteoritic impact melts have been derived from small impacts that failed to penetrate mafic-enriched near surface "mega-regolith" deposits overlying purer anorthositic crust (as suggested by Ohtake et al. 2009 to explain the relative rarity of exposed anorthosite on the surface).

Arai et al. (2008) have proposed that magnesian troctolitic lithologies, as sampled by the Dhofar 489 meteorite (Korotev et al. 2006; Takeda et al. 2006; Arai et al. 2008), may form an important component of the farside central Feldspathic Highlands Terrane (see also Pieters and Tompkins 1999; Lucey 2004; Warren et al. 2005; Lucey and Cahill 2006; Takeda et al. 2006). However, our results show no definitive evidence of feldspathic impact melt that has mixed with Dhofar 489-like magnesian ($>Mg\#_{80}$) troctolitic material. Therefore, we suggest that this rocktype is perhaps uncommon in the lunar highlands and future remote-sensing observations should be used to better confirm its occurrence and spatial distribution. One promising technique would be high spatial resolution X-ray fluorescence spectroscopy, which could be used to determine the stratigraphic variation of Fe/Mg within

the crust by determining the elemental compositions of central peaks and peak rings exhumed from a range of depths by impacts of a wide range of sizes (e.g., Crawford et al. 2009). Such observations would also help further constrain the launch localities of lunar meteorites, as discussed in Section Constraining the Source Region of DaG 400, MET 01210, PCA 02007, and MAC 88104/05.

In conclusion, if we assume that the four lunar meteorites of this study have sampled impact melted feldspathic crust in a minimum of four locations (i.e., one main site per meteorite: Table 2) and up to a maximum of nine locations (all feldspathic groups listed in Table 2), then our data set provides a new view of the variability of the lunar crust across the Moon from four to nine locations outside of the regions sampled by the Apollo and Luna missions (Figs. 11 and 12). Our data (Table 2) are consistent with other studies (Wieczorek and Zuber 2001; Korotev et al. 2003; Lucey et al. 2006 and references therein) that the lunar crust has variable lateral Mg/Fe ratios and contains regions that are ferroan troctolitic anorthosite normative, but more commonly are ferroan noritic anorthosite normative.

SUMMARY

MET 01210 is a basaltic regolith breccia that was consolidated in a mare region in close proximity to ferroan anorthosite outcrops (Day et al. 2006; Joy et al. 2008; Arai et al. 2010). DaG 400, PCA 02007, and MAC 88104/05 represent regoliths consolidated in more feldspathic regions of the Moon and could have been sourced from regoliths within the Feldspathic Highlands Terrane and the Outer Feldspathic Highlands Terrane (Figs. 11 and 12).

We have demonstrated the use of an in situ LA-ICP-MS sampling technique to conduct a high spatial resolution study of the minor and trace element composition of impact melt clast components within the brecciated lunar meteorite samples. Results of our study show:

1. Mafic impact melt geochemistry in MET 01210 shows mixing between feldspathic crust and an ITE-poor, Sc-rich, VLT/low-Ti mare basalt typically of the paired Y/A/M/M stones. The ITE-poor nature of the melt clasts indicates that the basalt target was KREEP-poor and located outside of the nearside Procellarum KREEP Terrane (Figs. 11 and 12).

2. Mafic impact melts in PCA 02007 and MAC 88104/05 also show mixing between KREEP-poor feldspathic crust and different types of low-Ti and VLT basalts. The presence of mafic impact melts in these meteorites, and rare basalt fragments, is consistent with other inferences that the FHT-O likely contains a fraction of buried VLT/low-Ti basalts, possibly in the form of cryptomaria (see also Terada et al. 2007b; Arai et al. 2010; Basilevsky et al. 2010).

3. Feldspathic impact melts and melt breccias have sampled feldspathic lunar crust in a minimum of four locations (i.e., one main site per meteorite as represented by the DaG type 2, MET type 1, PCA type 2, MAC type 2 groups: Table 2) and a maximum of nine locations (assuming that DaG 400 sampled at least three feldspathic sites, MET 01210 sampled one site, PCA 02007 sampled two sites and MAC 88104/05 sampled three sites: Table 2). These samples suggest that the lunar crust has lateral Mg# variations and is dominantly ferroan noritic anorthosite normative in nature.

4. Compared with feldspathic impact melts from the Apollo 16 mission (Korotev 1994), the four main groups of meteorite feldspathic impact melt have ITE-concentrations similar to the Apollo 16 group 4 feldspathic group. However, they are more mafic than these samples and have major element compositions more like the Apollo 16 group 3 varieties. In comparison to both Apollo 16 impact groups, the meteorite impact melts have notably lower Sr and Eu trace element concentrations (Fig. 10), indicating a lower plagioclase component.

5. We find no definitive evidence that any meteorite contains impact melt generated from melting magnesian ($Mg\#_{>80}$) troctolitic anorthosites, as represented material sampled by the Dhofar 489 meteorite and grouped stones (Korotev et al. 2006; Takeda et al. 2006; Arai et al. 2008).

Studies by current composition mapping instruments should provide a more detailed view of the compositional stratigraphy (Mg, Al, and Si) of the Feldspathic Highlands Terrane, thus helping to better constrain some of the key parameters needed to successfully geochemically model the composition of the lunar crust, and through it, a better understanding of lunar differentiation processes. These measurements will also help to constrain the source provenance of lunar meteorites.

Acknowledgments—Many thanks to Guy Consolmango and the Vatican Observatory for loaning the DaG 400 sample to the NHM and to MWG/NASA for the loan of Antarctic samples. Many thanks also to Mr. John Spratt (NHM), Dr. Sarah James (formally of the NHM), and Dr. Andy Beard (Birkbeck/UCL) for their assistance with analytical procedures. Many thanks for thorough reviews and helpful comments of Drs. Randy Korotev, James Day, Jeff Taylor, Barbara Cohen, Christian Koeberl, and an anonymous reviewer. We would like to acknowledge the resources made available

through the Lunar Meteorite List Website (Randy Korotev), the Lunar Meteorite Compendium (Kevin Righter), the Lunar Sample Compendium (Chuck Meyer), and the Virtual Moon Atlas. Thanks to the Leverhulme Trust, STFC, and LPI/NLSI for financial support. This is LPI contribution number 1600.

Editorial Handling—Dr. A. J. Timothy Jull

REFERENCES

Albee A. L., Quick J. E., and Chodos A. A. 1977. Source and magnitude of errors in "broad-beam analysis" (DBA) with the electron probe. 8th Lunar Science Conference. pp. 7–9.

Anders E. and Grevesse N. 1989. Abundances of the elements: Meteoritic and solar. *Geochimica et Cosmochimica Acta* 53:97–214.

Antonenko I., Head J. W., Mustard J. F., and Hawke B. R. 1995. Criteria for the detection of lunar cryptomaria. *Earth, Moon, and Planets* 69:141–172.

Arai T. and Warren P. 1999. Lunar meteorite Queen Alexandra Range 94281: Glass compositions and other evidence for launch pairing with Yamato-793274. *Meteoritics & Planetary Science* 34:209–234.

Arai T., Misawa K., and Kojima H. 2007. Lunar meteorite MIL 05035: Mare basalt paired with Asuka-881757 (abstract #1582). 38th Lunar and Planetary Science Conference. CD-ROM.

Arai T., Takeda H., Yamaguchi A., and Ohtake M. 2008. A new model of lunar crust: Asymmetry in crustal composition and evolution. *Earth, Planets and Space* 60:433–444.

Arai T., Hawke B. R., Giguere T. A., Misawa K., Miyamoto M., and Kojima H. 2010. Antarctic lunar meteorites Yamato-793169, Asuka-881757, MIL 05035, and MET 01210 (YAMM): Launch pairing and possible cryptomare origin. *Geochimica et Cosmochimica Acta* 74:2231–2248.

Arvidson R., Crozaz G., Drozd R. J., Hohenberg C. M., and Morgan C. J. 1975. Cosmic ray exposure ages of features and events at the Apollo landing sites. *Earth, Moon, and Planets* 13:259–276.

Basaltic Volcanism Study Project. 1981. *Basaltic volcanism on the terrestrial planets*. New York: Pergamon Press, Inc. 1286 p.

Basilevsky A. T., Neukum G., and Nyquist L. 2010. Lunar meteorites: What they tell us about the spatial and temporal distribution of mare basalts. (abstract #1214). 41st Lunar and Planetary Science Conference. CD-ROM.

Bland P. A., Alard O., Benedix G. K., Kearsley A. T., Menzies O. N., Watt L E., and Rogers N. W. 2005. Volatile fractionation in the early solar system and chondrule/matrix complementarity. *Proceedings of the National Academy of Sciences* 102:13755–13760.

Boyce J. M. and Johnson D. A. 1977. Ages of flow units in Mare Crisium based on crater density. Proceedings, 8th Lunar Science Conference. pp. 3495–3502.

Bukovanska M., Dobosi G., Brandstätter F., and Kurat G. 1999. Dar al Gani 400: Petrology and geochemistry of some major lithologies (abstract). *Meteoritics & Planetary Science* 34:A21.

Bussey D. B. J. and Spudis P. D. 2000. Compositional studies of the Orientale, Humorum, Nectaris, and Crisium lunar basins. *Journal of Geophysical Research* 105:4235–4243.

Cahill J. T., Floss C., Anand M., Taylor L. A., Nazarov M. A., and Cohen B. A. 2004. Petrogenesis of lunar highlands meteorites: Dhofar 025, Dhofar 081; Dar al Gani 262, and Dar al Gani 400. *Meteoritics & Planetary Science* 39:503–530.

Campbell B. A. and Hawke B. R. 2005. Radar mapping of lunar cryptomaria east of Orientale basin. *Journal of Geophysical Research* 110:E09002, doi:10.1029/2005JE002425.

Cohen B. A., Kring D. A., and Swindle T. D. 1999. Impact melt clasts in lunar meteorites Dar al Gani 262 and Dar al Gani 400 (abstract #5220). 62nd Annual Meteoritical Society Meeting.

Cohen B. A., James O. B., Taylor L. A., Nazarov M. A., and Barsukova L. D. 2004. Lunar highland meteorite Dhofar 026 and Apollo sample 15418: Two strongly shocked, partially melted, granulitic breccias. *Meteoritics & Planetary Science* 39:1419–1447.

Cohen B. A., Swindle T. D., and Kring D. A. 2005. Geochemistry and ^{40}Ar-^{39}Ar geochronology of lunar highland meteorite impact melt clasts. *Meteoritics & Planetary Science* 40:755–777.

Consolmagno G. J., Russell S. S., and Jeffries T. E. 2004. An in-situ study of REE abundances in three anorthositic impact melt lunar highland meteorites (abstract #1370). 35th Lunar and Planetary Science Conference. CD-ROM.

Crawford I. A., Joy K. H., Kellett B. J., Grande M., Anand M., Bhandari N., Cook A. C., d'Uston L., Fernandes V. A., Gasnault O., Goswami J., Howe C. J., Huovelin J., Koschny D., Lawrence D. J., Maddison B. J., Maurice S., Narendranath S., Pieters C., Okada T., Rothery D. A., Russell S. S., Sreekumar P., Swinyard B., Wieczorek M., and Wilding M. 2009. The scientific rationale for the C1XS X-Ray Spectrometer on India's Chandrayaan-1 mission to the Moon. *Planetary and Space Science* 57:725–734.

Crozaz G., Floss C., and Wadhwa M. 2003. Chemical alteration and REE mobilization in meteorites from hot and cold deserts. *Geochimica et Cosmochimica Acta* 67:4727–4741.

Day J. M. D., Floss C., Taylor L. A., Anand M., and Patchen A. D. 2006. Evolved mare basalt magmatism, high Mg/Fe feldspathic crust, chondritic impactors, and the petrogenesis of Antarctic lunar breccia meteorites Meteorite Hills 01210 and Pecora Escarpment 02007. *Geochimica et Cosmochimica Acta* 70:5957–5989.

Delano J. W. 1991. Geochemical comparison of impact glasses from lunar meteorites ALHA and MAC 88105 and Apollo 16 regolith 64001. *Geochimica et Cosmochimica Acta* 55:3019–3029.

Deutsch A. and Stöffler D. 1987. Rb-Sr-analyses of Apollo 16 melt rocks and a new age estimate for the Imbrium basin: Lunar basin chronology and the early heavy bombardment of the moon. *Geochimica et Cosmochimica Acta* 51:1951–1964.

Eugster O., Burger M., Krähenbühl U., Michel Th., Beer J., Hofmann H. J., Synal H. A., Woelfli W., and Finkel R. C. 1991. History of the paired lunar meteorites MAC 88104 and MAC 88105 derived from noble gas isotopes, radionuclides, and some chemical abundances. *Geochimica et Cosmochimica Acta* 55:3139–3148.

Fernandes V. A., Burgess R., and Morris A. 2009. ^{40}Ar-^{39}Ar age determinations of lunar basalt meteorites: Asuka 881757, Yamato 793169, Miller Range 05035, La Paz 02205, Northwest Africa 479 and Elephant Moraine 96008. *Meteoritics & Planetary Science* 44:805–821.

Floran R. J., Phinney W. C., Blanchard D. P., Warner J. L., Simonds C. H., Brown R. W., Brannon J. C., and Korotev

R. L. 1976. A comparison between the geochemistry and petrology of Apollo 16—Terrestrial impact melt analogs. 7th Lunar Science Conference. pp. 263–265.

Floss C. A., James A. B., McGee J. J., and Crozaz G. 1998. Lunar ferroan anorthosite petrogenesis: Clues from trace element distributions in FAN subgroups. *Geochimica et Cosmochimica Acta* 62:1255–1283.

Goodrich C. A. and Keil K. 1987. Mare basalts and other clasts in Yamato lunar meteorites Y-791197, -82192 and -82193. *Memoirs of National Institute of Polar Research, Special Issue* 46:56–70.

Goodrich C. A., Taylor G. J., Keil K., Boynton W. V., and Hill D. H. 1984. Petrology and chemistry of hyperferroan anorthosites and other clasts from lunar meteorite ALHA81005. Proceedings, 15th Lunar and Planetary Science Conference in *Journal of Geophysical Research* 89:C87–C94.

Haloda J., Týcová P., Korotev R. L., Fernandes V. A., Burgess R., Thöni M., Jelenc M., Jakeš P., Gabzdyl P., and Košler J. 2009. Petrology, geochemistry, and age of low-Ti mare-basalt meteorite Northeast Africa 003: A possible member of the Apollo 15 mare basaltic suite. *Geochimica et Cosmochimica acta* 73:3450–3470.

Haskin L. A., Helmke P. A., Blanchard D. P., Jacobs J. W., and Telander K. 1973. Major and trace element abundances in samples from the lunar highlands. Proceedings, 4th Lunar Science Conference. pp. 1275–1296.

Haskin L. A., Gillis J. J., Korotev R. L., and Jolliff B. L. 2000. The materials of the lunar Procellarum KREEP Terrane: A synthesis of data from geomorphological mapping, remote sensing, and sample analyses. *Journal of Geophysical Research* 105:20403–20415.

Hawke B. R., Spudis P. D., and Clark P. E. 1985. The origin of selected lunar geochemical anomalies: Implications for early volcanism and the formation of light plains. *Earth, Moon, and Planets* 32:257–273.

Hawke B. R., Gillis J. J., Giguere T. A., Blewett D. T., Lawrence D. J., Lucey P. G., Smith G. A., Spudis P. D., and Taylor G. J. 2005. Remote sensing and geologic studies of the Balmer-Kapteyn region of the Moon. *Journal of Geophysical Research* 110:E06004, doi:10.1029/2004JE002383.

Head III J. W. and Wilson L. 1992. Lunar mare volcanism - stratigraphy, eruption conditions, and the evolution of secondary crusts. *Geochimica et Cosmochimica Acta* 56:2155–2175.

Head III J. W., Melosh H. J., and Ivanov B. A. 2002. Martian meteorite launch: High-speed ejecta from small craters. *Science* 298:1752–1756.

Hiesinger H., Head III J. W., Wolf U., Jaumann R., and Neukum G. 2006. New ages for basalts in Mare Fecunditatis based on crater size-frequency measurements (abstract #1151). 37th Lunar and Planetary Science Conference. CD-ROM.

Hörz F., Grieve R., Heiken G., Spudis P., and Binder A. 1991. Lunar surface processes. In *Lunar sourcebook*, edited by Heiken G., Vaniman D., and French B. M. Cambridge: Cambridge University Press. pp. 1–120.

James O. B., Lindstron M. M., and Flohr M. K. 1989. Ferroan anorthosite from lunar breccia 64435: Implications for the origin and history of lunar ferroan anorthosites. Proceedings, 19th Lunar and Planetary Science Conference. pp. 219–243.

Jolliff B. L. 1998. Large-Scale Separation of K-frac and REEP-frac in the source regions of Apollo impact-melt breccias, and a revised estimate of the KREEP composition. *International Geology Review* 40:916–935.

Jolliff B. L. and Haskin L. A. 1995. Cogenetic rock fragments from a lunar soil: Evidence of a ferroan noritic-anorthosite pluton on the Moon. *Geochimica et Cosmochimica Acta* 59:2345–2374.

Jolliff B. L., Korotev R. L., and Haskin L. A. 1991. A ferroan region of the lunar highlands as recorded in meteorites MAC 88104 and MAC 88105. *Geochimica et Cosmochimica Acta* 55:3051–3071.

Jolliff B. L., Gillis J. J., Haskin L. A., Korotev R. L., and Wieczorek M. A. 2000. Major lunar crustal terranes: Surface expressions and crust-mantle origins. *Journal of Geophysical Research* 105:4197–4216.

Jolliff B. L., Wieczorek M. A., Shearer C. K., and Neal C. R. 2006. New views of the moon. *Reviews in Mineralogy and Geochemistry* 60:i–xxii and 772.

Joy K. H. 2007. Studies in lunar geology and geochemistry using sample analysis and remote sensing measurements. Ph.D. thesis, University of London, London, UK.

Joy K. H., Crawford I. A., Russell S. S., Swinyard B., Kellett B., and Grande M. 2006a. Lunar regolith breccias MET 01210, PCA 02007 and DAG 400: Their importance in understanding the lunar surface and implications for the scientific analysis of D-CIXS data (abstract #1274). 37th Lunar and Planetary Science Conference. CD-ROM.

Joy K. H., Crawford I. A., Downes H., Russell S. S., and Kearsley A. T. 2006b. A petrological, mineralogical and chemical analysis of the lunar mare basalt meteorites LaPaz Icefield 02205, 02224, and 02226. *Meteoritics & Planetary Science* 41:1003–1026.

Joy K. H., Crawford I. A., Anand M., Anand M., Greenwood R. C., Franchi I. A., and Russell S. S. 2008. The petrogenesis of Miller Range 05035: A new lunar gabbroic meteorite. *Geochimica et Cosmochimica Acta* 72:3822–3844.

Kempa M. J. and Papike J. J. 1980. The Apollo 16 regolith—Comparative petrology of the greater than 20 micron and 20-10 micron soil fractions, lateral transport and differential volatilization. Proceedings, 11th Lunar and Planetary Science Conference. pp. 1635–1661.

Koeberl C., Warren P. H., Lindstrom M. M., Spettel B., and Fukuoka T. 1989. Preliminary examination of the Yamato-86032 lunar meteorite: II. Major and trace element chemistry. *Proceedings of the NIPR Symposium on Antarctic Meteorites* 2:15–24.

Koeberl C., Kurat G., and Brandstätter F. 1991. MAC 88105-A regolith breccia from the lunar highlands: Mineralogical, petrological, and geochemical studies. *Geochimica et Cosmochimica Acta* 55:3073–3087.

Korotev R. L. 1994. Compositional variation in the Apollo 16 impact-melt breccias and inferences for the geology and bombardment history of the Central Highlands of the Moon. *Geochimica et Cosmochimica Acta* 58:3931–3969.

Korotev R. L. 1996. On the relationship between the Apollo 16 ancient regolith breccias and feldspathic fragmental breccias, and the composition of the prebasin crust in the Central Highlands of the Moon. *Meteoritics & Planetary Science* 31:403–412.

Korotev R. L. 1997. Invited review: Some things we can infer from the Moon from the composition of the Apollo 16 regolith. *Meteoritics & Planetary Science* 32:447–478.

Korotev R. L. 2000. The great lunar hot spot and the composition and origin of the Apollo mafic (''LKFM'') impact-melt breccias. *Journal of Geophysical Research* 105:4317–4345.

Korotev R. L. 2005. Lunar geochemistry as told by lunar meteorites. *Chemie der Erde* 65:297–346.

Korotev R. L., Jolliff B. L., and Rockow K. M. 1996. Lunar meteorite Queen Alexandra Range 93069 and the iron concentration of the lunar highlands surface. *Meteoritics & Planetary Science* 31:909–924.

Korotev R. L., Jolliff B. L., Zeigler R. A., Gillis J. J., and Haskin L. A. 2003. Feldspathic lunar meteorites and their implications for compositional remote sensing of the lunar surface and the composition of the lunar crust. *Geochimica et Cosmochimica Acta* 67:4895–4923.

Korotev R. L., Zeigler R. A., and Jolliff B. L. 2006. Feldspathic lunar meteorites Pecora Escarpment 02007 and Dhofar 489: Contamination of the surface of the lunar highlands by post-basin impacts. *Geochimica et Cosmochimica Acta* 70:5935–5956.

Korotev R. L., Irving A. J., and Bunch T. E. 2008. Keeping up with the lunar meteorites—2008 (abstract #1209). 34th Lunar and Planetary Science Conference. CD-ROM.

Korotev R. L., Zeigler R. A., Jolliff B. L., Irving A. J., and Bunch T. E. 2009. Brecciated lunar meteorites of intermediate iron concentration. *Meteoritics & Planetary Science* 44:1287–1322.

Lawrence D. J., Feldman W. C., Elphic R. C., Little R. C., Prettyman T. H., Maurice S., Lucey P. G., and Binder A. B. 2002. Iron abundances on the lunar surface as measured by the Lunar Prospector gamma-ray and neutron spectrometers. *Journal of Geophysical Research* 107:5130, doi:10.1029/2001JE001530.

Lawrence D. J., Elphic R. C., Feldman W. C., Prettyman T. H., Gasnault O., and Maurice S. 2003. Small-area thorium features on the lunar surface. *Journal of Geophysical Research* 108:5102, doi:10.1029/2003JE002050.

Levine J., Becker T. A., Muller R. A., and Renne P. R. 2005. $^{40}Ar/^{39}Ar$ dating of Apollo 12 impact spherules. *Geophysical Research Letters* 32:L15201, doi:10.1029/2005GL022874.

Lindstrom D. J. 1999. Accuracy of rastered-beam analysis (RBA) of lunar breccia clasts by electron microprobe (abstract #1917). 30th Lunar and Planetary Science Conference. CD-ROM.

Lindstrom M. M. and Salpas P. A. 1982. Geochemical studies of rocks from North Ray crater. Proceedings, 12th Lunar and Planetary Science Conference. pp. 305–322.

Lindstrom M. M., Lindstrom D. J., Korotev R. L., and Haskin L. A. 1986. Lunar meteorite Yamato-791197: A polymict anorthositic norite from the lunar highlands. *Memoirs of National Institute of Polar Research, Special Issue* 41:58–75.

Lindstrom M. M., Wentworth S. J., Martinez R. R., Mittlefehldt D. W., McKay D. S., Wang M.-S., and Lipschutz M. J. 1991. Geochemistry and petrography of the MacAlpine Hills lunar meteorites. *Geochimica et Cosmochimica Acta* 55:3089–3103.

Liu Y., Floss C., Day J. M. D., Hill E., and Taylor L. A. 2009. Petrogenesis of lunar mare basalt meteorite Miller Range 05035. *Meteoritics & Planetary Science* 44:261–284.

Longhi J. 2003. A new view of lunar ferroan anorthosites: Postmagma ocean petrogenesis. *Journal of Geophysical Research* 108:5083, doi:10.1029/2002JE001941.

Lucey P. G. 2004. Mineral maps of the Moon. *Geophysical Research Letters* 3:L08701, doi:10.1029/2003GL019406.

Lucey P. G. and Cahill J. 2006. Magnesian rock types in the lunar highlands: Remote sensing using data from Lunar Prospector and Clementine (abstract #1660). 37th Lunar and Planetary Science Conference. CD-ROM.

Lucey P. G., Blewett D. T., and Jolliff B. L. 2000. Lunar iron and titanium abundance algorithms based on final processing of Clementine UVVIS images. *Journal of Geophysical Research* 105:20297–20305.

Lucey P., Korotev R. L., Gillis J. J., Taylor L. A., Lawrence D., Campbell B. A., Elphic R., Feldmann B., Hood L. L., Hunten D., Mendillo M., Noble S., Papike J J., Reedy R. C., Lawson S., Prettyman T., Gasault O., and Maurice S. 2006. Understanding the lunar surface and Space-Moon interactions. In *New views of the Moon*, edited by Jolliff B. L., Wieczorek M. A., Shearer C. K. and Neal C. R. Reviews in Mineralogy and Geochemistry, vol. 60. Chantilly, VA: Mineralogical Society of America. pp 83–219.

McKay D. S., Morris R. V., Dungan M. A., Fruland R. M., and Fuhrman R. 1976. Comparative studies of grain size separates of 60009. Proceedings, 7th Lunar Science Conference. pp. 295–313.

McKay D. S., Bogard D. D., Morris R. V., Korotev R. L., Johnson P., and Wentworth S. J. 1986. Apollo 16 regolith breccias: Characterization and evidence for early formation in the mega-regolith. Proceedings, 16th Lunar and Planetary Science Conference. *Journal of Geophysical Research* 91:D277–D303.

McKay D. S., Heiken G., Basu A., Blanford G., Simon S., Reedy R., French B. M., and Papike J. 1991. The lunar regolith. In *Lunar sourcebook*, edited by Heiken G., Vaniman D. and French B. M. Cambridge: Cambridge University Press. pp. 286–356.

McKinley J. P., Taylor G. J., Keil K., Ma M.-S., and Schmitt R. A. 1984. Apollo 16: Impact melt sheets, contrasting nature of the Caylay Plains and Descartes Mountains, and geologic history. *Journal of Geophysical Research* 89:B513–B524.

Naney M. T., Crowl D. M., and Papike J. J. 1976. The Apollo 16 drill core—Statistical analysis of glass chemistry and the characterization of a high alumina-silica poor/HASP/glass. Proceedings, 7th Lunar Science Conference. pp. 155–184.

Neal C. R. and Kramer G. Y. 2006. The petrogenesis of the Apollo 14 high-Al mare basalts. *American Mineralogist* 91:1521–1535.

Neal C. R., Taylor L. A., Liu Y., and Schmitt R. A. 1991. Paired lunar meteorites MAC 88104 and MAC 88105: A new ''FAN'' of lunar petrology. *Geochimica et Cosmochimica Acta* 55:3037–3049.

Nishiizumi K. and Caffee M. W. 2001. Exposure histories of lunar meteorites Dhofar 025, 026, and Northwest Africa 482 (abstract #5411). 64th Meteoritical Society Meeting.

Nishiizumi K., Arnold J. R., Klein J., Fink D., Middleton R., Kubik P. W., Sharma P., Elmore D., and Reedy R. C. 1991. Exposure histories of lunar meteorites: ALHA81005, MAC88104, MAC88105, and Y791197. *Geochimica et Cosmochimica Acta* 55:3149–3155.

Nishiizumi K., Hillegonds D. J., and Welten K. C. 2006. Exposure and terrestrial histories of lunar meteorites LAP

02205/02224/02226/02436, MET 01210, and PCA 02007 (abstract #2369). 37th Lunar and Planetary Science Conference. CD-ROM.

Norman M. D., Griffin W. L., Pearson N. J., Garcia M. O., and O'Reilly S. Y. 1998. Quantitative analysis of trace element abundances in glasses and minerals: A comparison of laser ablation inductively coupled plasma mass spectrometry, solution inductively coupled plasma mass spectrometry, proton microprobe and electron microprobe data. *Journal of Analytical Atomic Spectrometry* 13:477–482.

Nyquist L., Bogard D., Yamaguchi A., Shih C.-Y., Karouji Y., Ebihara M., Reese Y., Garrison D., McKay G., and Takeda H. 2006. Feldspathic clasts in Yamato-86032: Remnants of the lunar crust with implications for its formation and impact history. *Geochimica et Cosmochimica Acta* 70:5990–6015.

Ohtake M., Matsunaga T., Haruyama J., Yokota Y., Morota T., Honda C., Ogawa Y., Torii M., Miyamoto H., Arai T., Hirata N., Iwasaki A., Nakamura R., Hiroi T., Sugihara T., Takeda H., Otake H., Pieters C. M., Saiki K., Kitazato K., Abe M., Asada N., Demura H., Yamaguchi Y., Sasaki S., Kodama S., Terazono J., Shirao M., Yamaji A., Minami S., Akiyama H., and Josset J. 2009. The global distribution of pure anorthosite on the Moon. *Nature* 461:236–240.

Palme H., Spettel B., Jochum K. H., Dreibus G., Weber H., Weckwerth G., Wänke H., Bischoff A., and Stöffler D. 1991. Lunar highland meteorites and the composition of the lunar crust. *Geochimica et Cosmochimica Acta* 55:3105–3122.

Papike J. J., Spilde M. N., Adcock C. T., Fowler G. W., and Shearer C. K. 1997. Trace-element fractionation by impact-induced volatilization: SIMS study of lunar HASP samples. *American Mineralogist* 82:630–634.

Papike J. J., Ryder G., and Shearer C. K. 1998. Chapter 5. Lunar samples. In *Planetary materials*, edited by Papike J. J. Reviews in Mineralogy, vol. 36. Washington, D.C.: Mineralogical Society of America. pp. 5.1–5.234.

Pearce N. J. G., Perkins W. T., Westgate J. A., Gorton M. P., Jackson S. E., Neal C. R., and Chenery S. P. 1997. New data for the National Institute of Standards and Technology 610 and 612 glass reference materials. *Geostandards Newsletter* 21:115–144.

Pieters C. M. and Tompkins S. 1999. Tsiolkovsky crater: A window into crustal processes on the lunar farside. *Journal of Geophysical Research* 104:21935–21949.

Powell B. N., Dungan M. A., and Weiblen P. W. 1975. Apollo 16 feldspathic melt rocks: Clues to the magmatic history of the lunar crust. Proceedings, 6th Lunar Science Conference. pp. 415–433.

Prettyman T. H., Hagerty J. J., Elphic R. C., Feldman W. C., Lawrence D. J., McKinney G. W., and Vaniman D. T. 2006. Elemental composition of the lunar surface: Analysis of gamma ray spectroscopy data from Lunar Prospector. *Journal of Geophysical Research—Planets*. 111:E12007, doi:10.1029/2005JE002656.

Reimold W. U., Nyquist L. E., Bansal B. M., Wooden J. L., Shih C.-Y., and Weismann H. 1985. Isotope analysis of crystalline impact melt rocks from Apollo 16 stations 11 and 13, North Ray Crater. *Journal of Geophysical Research Sup* 90:C431–C448.

Robinson K. L. and Treiman A. H. 2010. Mare basalt fragments in lunar highlands meteorites: Connecting measured Ti abundances with orbital remote sensing (abstract #1788). 41st Lunar and Planetary Science Conference. CD-ROM.

Rubin A. E. 1997. The Hadley Rille enstatite chondrite and its agglutinate-like rim: Impact melting during accretion to the Moon. *Meteoritics & Planetary Science* 32:135–141.

Russell S. S., Folco L., Grady M. M., Zolensky M. E., Jones R., Righter K., Zipfel J., and Grossman J. N. 2004. The Meteoritical Bulletin, No. 88. *Meteoritics & Planetary Science* 39:A215–A272.

Ryder G. 1985. *Apollo 15 lunar sample information catalog part 2: 15306-15468*. Publication: JSC-20787. Houston, Texas: Lyndon B. Johnson Space Center.

Ryder G. and Spudis P. 1994. Chemical composition and origin of Apollo 15 impact melts. *Journal of Geophysical Research* 92:E432–E446.

Schnare D. W., Day J. M. D., Norman M. D., Liu Y., and Taylor L. A. 2008. A laser-ablation ICP-MS study of Apollo 15 low-titanium olivine-normative and quartz-normative mare basalts. *Geochimica et Cosmochimica Acta* 72:2556–2572.

Shearer C. K. and Floss C. 2000. Evolution of the Moon's mantle and crust as reflected in trace-element microbeam studies of lunar magmatism. In *Origin of the Earth and Moon*, edited by Canup R. M., Righter K. and 69 collaborating authors. Tucson, AZ: The University of Arizona Press. pp. 339–359.

Shearer C. K., Hess P. C., Wieczorek M. A., Pritchard M. E., Parmentier E. M., Borg L., Longhi J., Elkins-Tanton L. T., Neal C. R., Antonenko I., Canup R. M., Halliday A. N., Grove T. L., Hager B. H., Less D.-C., and Wiechert U. 2006. Thermal and magmatic evolution of the Moon. In *New views of the Moon*, edited by Jolliff B. L., Wieczorek M. A., Shearer C. K. and Neal C. R. Reviews in Mineralogy and Geochemistry 60:365–518.

Simonds C. H., Warner J. L., and Phinney W. C. 1973. Petrology of Apollo 16 poikilitic rocks. Proceedings, 4th Lunar Science Conference. pp. 613–632.

Simonds C. H., Phinney W. C., Warner J. L., McGee P. E., Geeslin J., Brown R. W., and Rhodes J. M. 1977. Apollo 14 revisited, or breccias aren't so bad. Proceedings, 8th Lunar Science Conference. pp. 1869–1893.

Sokol A. K., Fernandes V. A., Schulz T., Bischoff A., Burgessc R., Clayton R. N., Münker C., Nishiizumi K., Palme H., Schultz L., Weckwerth G., Mezger K., and Horstmannaan M. 2008. Geochemistry, petrology and ages of the lunar meteorites Kalahari 008 and 009: New constraints on early lunar evolution. *Geochimica et Cosmochimica Acta* 72:4845–4873.

Spudis P. D. 1984. Apollo 16 site geology and impact melts: Implications for the geologic history of the lunar highlands. *Journal of Geophysical Research* 89:C95–C107.

Spudis P. D. 1993. Chapter 8. Multi-ringed basins on the terrestrial planets. In *The geology of multi-ring impact basins: The Moon and other planets*. Cambridge: Cambridge University Press. pp. 165–190.

Spudis P. D. and Davis P. A. 1986. A chemical and petrological model of the lunar crust and implications for lunar crustal origin. *Journal of Geophysical Research* 91:E84–E90.

Spudis P. D., Hawke B. R., Taylor G. J., McCormick K. A., Keil K., and Grieve R. A. F. 1991. Sources of mineral fragments in impact melts 15445 and 15455: Toward the origin of low-K Fra Mauro basalt. Proceedings, 21st Lunar and Planetary Science Conference. pp. 151–165.

Stöffler D., Knoll H.-D., Marvin U. B., Simonds C. H., and Warren P. H. 1980. Recommended classification and nomenclature of lunar highland rocks—A committee report. Proceedings, Conference Lunar Highlands Crust. pp. 51–70.

Stöffler D., Ryder G., Ivanov B. A., Artemieva N. A., Cintala M. J., and Grieve R. A. F. 2006. Cratering history and lunar chronology. In *New views of the Moon*, edited by Jolliff B. L., Wieczorek M. A., Shearer C. K. and Neal C. R. *Reviews in Mineralogy and Geochemistry* 60:519–596.

Swindle T. D., Spudis P. D., Taylor G. J., Korotev R. L., Nichols R. H., and Olinger C. T. 1991. Searching for crisium basin ejecta: Chemistry and ages of Luna 20 impact melts. Proceedings, 21st Lunar and Planetary Science Conference. pp. 167–181.

Swinyard B. M., Joy K. H., Kellett B. J., Crawford I. A., Grande M., Howe C. J., Gasnault O., Fernandes V. A., Lawrence D. J., Russell S. S., Wieczorek M. A., Foing B. H., and the SMART-1 team. 2009. X-ray fluorescence observations of the Moon by SMART-1/D-CIXS and the first detection of Ti Kα from the lunar surface. *Planetary and Space Science* 57:744–750.

Takeda H., Yamaguchi A., Bogard D. D., Karouji Y., Ebihara M., Ohtake M., Saiki K., and Arai T. 2006. Magnesian anorthosites and a deep crustal rock from the farside crust of the Moon. *Earth and Planetary Science Letters* 247:171–184.

Taylor G. J. 1991. Impact melts in the MAC 88105 lunar meteorite: Inferences for the lunar magma ocean hypothesis and the diversity of basaltic impact melts. *Geochimica et Cosmochimica Acta* 55:3031–3036.

Taylor G. J., Warren P., Ryder G., Delano J., Pieters C., and Lofgren G. 1991. Lunar rocks. In *Lunar sourcebook*, edited by Heiken G., Vaniman D. and French B. M. Cambridge: Cambridge University Press. pp. 183–284.

Terada K., Sasaki Y., Anand M., Joy K. H., and Sano Y. 2007a. Uranium-lead systematics of phosphates in lunar basaltic regolith breccia, Meteorite Hills 01210. *Earth and Planetary Science Letters* 259:77–84.

Terada K., Anand M., Sokol A. K., Bischoff A., and Sano Y. 2007b. Cryptomare magmatism 4.35 Gyr ago recorded in lunar meteorite Kalahari 009. *Nature* 450:849–853.

Vaniman D. T. and Bish D. L. 1990. Yoshiokaite, a new Ca,Al-silicate mineral from the Moon. *American Mineralogist* 75:676–686.

Warren P. H. 1989. KREEP: Major-element diversity, trace-element uniformity (Almost). In *Workshop on moon in transition: Apollo 14, KREEP, and evolved lunar rocks*, edited by Taylor G. J. and Warren P. H. LPI Technical Report 89-03, published by Lunar and Planetary Institute. pp. 149.

Warren P. H. 1994. Lunar and Martian meteorite delivery systems. *Icarus* 111:338–363.

Warren P. H. 1997. The unequal host-phase density effect in electron probe defocused beam analysis: An easily correctable problem (abstract #1497). Proceedings, 28th Lunar and Planetary Science Conference.

Warren P. H. 2005. "New" lunar meteorites: Implications for composition of the global lunar surface, lunar crust, and the bulk Moon. *Meteoritics & Planetary Science* 40:335–511.

Warren P. H. and Wasson J. T. 1977. Pristine nonmare rocks and the nature of the lunar crust. Proceedings, 8th Lunar Science Conference. pp. 2215–2235.

Warren P. H. and Kallemeyn G. W. 1987. Geochemistry of lunar meteorite Yamato-82192: Comparison with Yamato-791197, ALHA81005, and other lunar samples. *Memoirs of National Institute of Polar Research, Special Issue* 46:3–20.

Warren P. H. and Wasson J. T. 1978. Compositional-petrographic investigation of pristine nonmare rocks. Proceedings, 9th Lunar and Planetary Science Conference. pp. 185–217.

Warren P. H., Ulff-Møller F., and Kallemeyn G. W. 2005. "New" lunar meteorites: Impact melt and regolith breccias and large-scale heterogeneities of the upper lunar crust. *Meteoritics & Planetary Science* 40:477–506.

Wasson J. T. and Kallemeyn G. W. 1988. Compositions of chondrites. *Philosophical Transactions of the Royal Society of London Series A* 325:535–544.

Wentworth S. J. and McKay D. S. 1990. Lunar meteorite MAC 88104/5: Petrography and glass compositions. Proceedings, 21st Lunar and Planetary Science Conference. pp. 1323–1324.

Wentworth S., Taylor G. J., Warner R. D., Keil K., Ma M.-S., and Schmitt R. A. 1979. The unique nature of Apollo 17 VLT mare basalts. Proceedings, 10th Lunar and Planetary Science Conference. pp. 207–223.

Wieczorek M. A. and Zuber M. T. 2001. The composition and origin of the lunar crust: Constraints from central peaks and crustal thickness modeling. *Geophysical Research Letters* 28:4023–4026.

Wieczorek M. A., Jolliff B. L., Khan A., Pritchard M. E., Weiss B. P., Williams J. G., Hood L. L., Righter K., Neal C. R., Shearer C. K., McCallum I. S., Tompkins S., Hawke B. R., Peterson C., Gillis J. J., and Bussey B. 2006. The constitution and structure of the lunar interior. In *New views of the Moon*, edited by Jolliff B. L., Wieczorek M. A., Shearer C. K. and Neal C. R. *Reviews in Mineralogy and Geochemistry* 60:221–364.

Yanai K., Takeda H., Lindstrom M. M., Tatsumoto M., Torigoe N., Misawa K., Warren P. H., Kallemeyn G. W., Koeberl C., and Kojima H. 1993. Consortium reports on lunar meteorites Yamato-793169 and Asuka-881757, a new type of mare basalt. Proceedings, 24th Lunar and Planetary Science Conference. pp. 1555–1556.

Zipfel J., Spettel B., Palme H., Wolf D., Franchi I., Sexton A. S., Pillinger C. T., and Bischoff A. 1998. Dar al Gani 400: Chemistry and petrology of the largest lunar meteorite (abstract). *Meteoritics & Planetary Science* 33:A171.

Zolensky M. E. 1997. Structural water in the Bench crater chondrite returned from the Moon. *Meteoritics & Planetary Science* 32:15–18.

SUPPORTING INFORMATION

Additional supporting information may be found in the online version of this article:

Table S1. Major (wt%), minor and trace bulk (ppm) composition of impact melt and melt breccias in DaG 400, MET 01210, PCA 02007 and MAC 88104/05.

Please note: Wiley-Blackwell is not responsible for the content or functionality of any supporting materials supplied by the authors. Any queries (other than missing material) should be directed to the corresponding author for the article.